Hotspot Formation and Dynamics for a Continuum Model of Urban Crime

W. H. TSE, M. J. WARD

Wang Hung Tse, Michael Ward; Department of Mathematics, Univ. of British Columbia, Vancouver, B.C., V6T 1Z2, Canada.

(*Received 29 May 2015*)

The existence, stability, and dynamics of localized patterns of criminal activity are studied for the reaction-diffusion model of urban crime introduced by Short et. al. [Math. Models. Meth. Appl. Sci., **18**, Suppl. (2008), pp. 1249–1267]. In the singularly perturbed limit of small diffusivity ratio, this model admits hotspot patterns, where criminal activity of high amplitude is localized within certain narrow spatial regions. By using a combination of asymptotic analysis and numerical path-following methods, hotspot equilibria are constructed on a finite 1-D domain and their bifurcation properties analyzed as the diffusivity of criminals is varied. It is shown, both analytically and numerically, that new hotspots of criminal activity can be nucleated in low crime regions with inconspicuous crime activity gradient when the spatial extent of these regions exceeds a critical threshold. These nucleations are referred to as "peak insertion" events, and for the steady-state problem they occur near a saddle-node bifurcation point characterizing hotspot equilibria. For the time-dependent problem, a differential algebraic (DAE) system characterizing the slow dynamics of a collection of hotspots is derived, and the results compared favorably with full numerical simulations of the PDE system. The asymptotic theory to construct hotspot equilibria, and to derive the DAE system for quasi-steady patterns, is based on the resolution of a triple-deck structure near the core of each hotspot and the identification of so-called switchback terms.

Keywords: Matched asymptotic expansions, nonlocal eigenvalue problem, fold point, peak insertion, slow hotspot dynamics, switchback term, renormalization.

1 Introduction

In recent years there has been a significant focus on develop mathematical tools to understand and predict spatial patterns of urban crime (cf. [**32**, **33**, **34**]). One main impetus underlying this effort is the increased availability of residential burglary data, which indicates that high levels of crime are often concentrated in certain spatial regions, known as hotspots, that can evolve over time [**2**]. Many studies have hypothesized that such hotspots are due to a repeat or near-repeat victimization effect, which postulates that crime in a certain region induces more crime in that and nearby regions (cf. [**16**], [**39**]).

In [**32**] and [**34**] an agent-based model of urban crime that takes into account repeat or near-repeat victimization was formulated, and its continuum limit derived. In dimensionless form, the continuum limit of this agent-based model on a 1-D domain $|x| \le \ell$ is the two-component reaction-diffusion (RD) system

$$A_t = \epsilon^2 A_{xx} - A + \rho A + \alpha\,, \qquad \rho_t = D\left(\rho_x - \frac{2\rho}{A}A_x\right)_x - \rho A + \gamma - \alpha\,, \tag{1.1}$$

with no-flux boundary conditions $\rho_x = A_x = 0$ at $x = \pm\ell$. Here, $\rho(x,t)$ is the density of criminals, $A(x,t)$ is the "attractiveness" of the environment to burglary, and the chemotactic drift term $-2D\left(\rho A_x/A\right)_x$ models the tendency of criminals to move towards sites with a higher attractiveness. In addition, $\alpha > 0$ is the constant baseline attractiveness, while $\gamma - \alpha$, with $\gamma > \alpha$, models a constant rate of re-introduction of criminals after a burglary. The constants $D > 0$ and $\epsilon^2 > 0$, with $\epsilon \ll 1$, are the diffusivities of the criminal density and attractiveness, respectively. Further details of the model are given in [**32**].

We remark that by the simple rescaling $\tilde{x} = x/\sqrt{D}$, (1.1) can be recast to the interval $(-\ell/\sqrt{D}, \ell/\sqrt{D})$, with the new diffusivities $\tilde{\epsilon} = \epsilon/\sqrt{D}$ and $\tilde{D} = 1$. This recovers the system given in [**32**] without the factor D. However, in our analysis, rather than using the domain length as a bifurcation parameter, we will consider (1.1) on a fixed domain,

but allow the criminal diffusivity $D = \mathcal{O}(1)$ to vary while treating the diffusivity ϵ^2 of the attractiveness field as an asymptotically small quantity.

The system (1.1) has the unique spatially homogeneous steady-state $A_e = \gamma$, and $\rho_e = 1 - \alpha/\gamma > 0$. The linear stability analysis of [**34**] showed that this solution is linearly unstable in the limit $\epsilon \to 0$ when

$$\gamma > \frac{3}{2}\alpha\,, \tag{1.2}$$

and that a spatially heterogeneous solution bifurcates from the spatially homogeneous steady-state at the bifurcation point $\gamma \sim \frac{3}{2}\alpha$ when $\epsilon \to 0$. Moreover, the weakly nonlinear analysis of [**33**] showed that this Turing bifurcation is subcritical when $\epsilon \ll 1$ (see also Fig. 7 of [**21**]).

Although weakly nonlinear theory, based on a normal form equation derived from a multiple-scales approximation, is able to characterize the development of spatial patterns near the Turing bifurcation point, it is not capable of describing the highly localized spatial patterns observed in full numerical simulations of (1.1) when the parameter values are not near the Turing point. More specifically, an initial random perturbation close to an unstable spatially homogeneous steady-state typically leads to highly localized spatial patterns, consisting of the concentration of criminal activity in localized spatial regions. We refer to such patterns as hotspot patterns. A localized hotspot solution, not amenable to an analytical description by a weakly nonlinear analysis, was observed in the numerical solutions of [**33**].

To illustrate these hotspot patterns, we perform full numerical simulations of (1.1) using the software `PDEPE` in `MATLAB R2013b`. For $\epsilon = 0.05$, $D = 2$, $\gamma = 2$, and $\alpha = 1$, in the right panel of Fig. 1 we plot A and ρ at some large time when the initial condition is a small random perturbation of the unstable spatially uniform state as shown in the left panel of Fig. 1. Since $\gamma > 3\alpha/2$, the spatially uniform state is unstable and we observe, for large time, that the solution approaches a steady-state pattern with one interior hotspot. For the same parameter set, but where the initial condition for A has two localized bumps, in Fig. 2 we show the initial formation of a two-hotpot pattern on an $\mathcal{O}(1)$ time-scale, followed by a very slow dynamics of the two-hotspot pattern towards its steady-state limit. One of the main goals of this paper is to give an explicit analytical characterization of the slow dynamics of such quasi-steady state hotspot patterns.

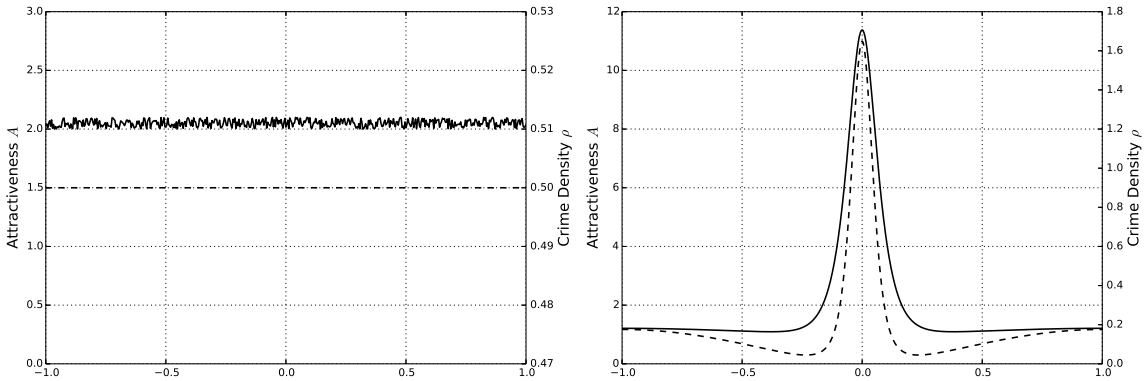

Figure 1. A Turing instability leading to a localized steady-state solution. Parameter values are $\epsilon = 0.05$, $D = 2$, $\ell = 1$, $\gamma = 2$, $\alpha = 1$, so that $\gamma > 3\alpha/2$. The initial condition (left panel) for the numerical solution of (1.1) is a small random perturbation of the spatially uniform state given by $A(x,0) = A_e + \text{rand} * 0.1$, $\rho(x,0) = \rho_e$, where $A_e = \gamma = 2$ and $\rho_e = 1 - \alpha/\gamma = 0.5$. The right panel shows the hotspot solution at the final time $t = 10^5$ with A (solid curve) and ρ (dotted curve). Notice that the range of A and ρ are on different scales.

In addition to [**32**, **33**, **34**], there have been a few other previous studies on pattern formation properties of the crime model (1.1). For the parameter regime $D \gg 1$, hotspot equilibria and their stability properties were analyzed in [**21**] by using a combination of formal asymptotic methods and results from the spectral theory of nonlocal eigenvalue problems. In [**1**] the existence of these hotspot equilibria for the regime $D \gg 1$ was established rigorously using a Lyapunov-Schmidt reduction. In [**31**] the local existence of solutions to the crime model in multi-dimensional domains was established. In [**5**] the branching behavior near the Turing point associated with the spatially homogeneous

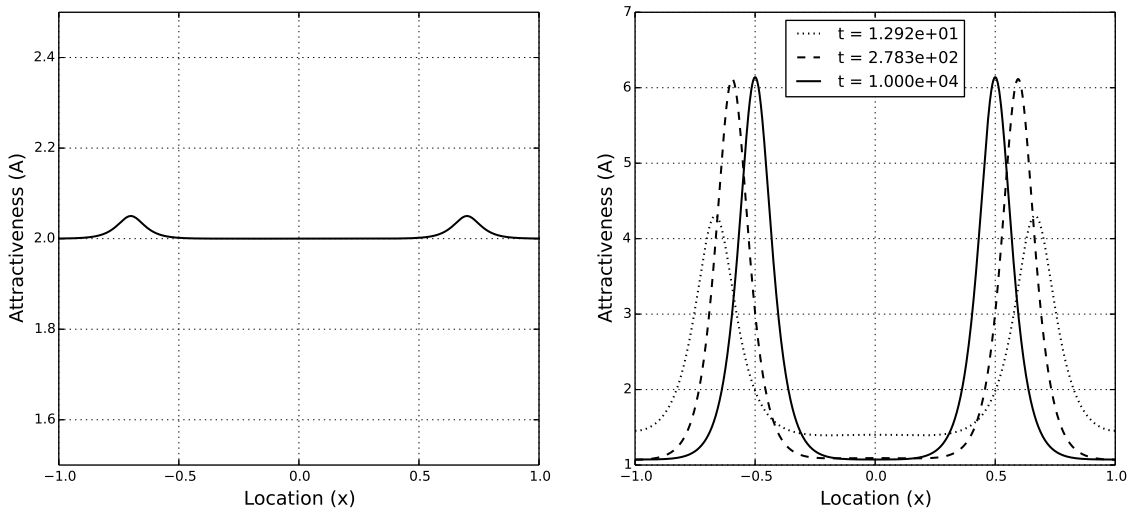

Figure 2. Small initial bumps in A quickly evolve into hotspots, which then move slowly to their steady-state locations. Parameter values are $\epsilon = 0.05$, $D = 2$, $\ell = 1$, $\gamma = 2$, $\alpha = 1$, so that $\gamma > 3\alpha/2$. The initial condition (left panel) for the numerical solution of (1.1) is $A(x,0) = A_e + \epsilon \sum_{i=1}^{2} \mathrm{sech}(\frac{x-x_{0,i}}{\epsilon})$ and $\rho(x,0) = \rho_e$, where $x_{0,1} = -0.7$, $x_{0,2} = 0.7$, $A_e = \gamma = 2$, and $\rho_e = 1 - \alpha/\gamma = 0.5$. We only plot A.

steady-state is characterized rigorously. Similar bifurcation theoretic results characterizing branching behavior from the spatially homogeneous steady-state for some extensions of the basic crime model (1.1) are given in [**13**].

In addition to [**21**], the previous work that is most relevant to our study is that of [**26**]. For $D = 1$, in [**26**] bifurcation software was used to numerically show that there is an intricate homoclinic snaking bifurcation structure for the steady-states of (1.1) on the infinite line when the parameter γ is below the Turing bifurcation threshold γ_c, for which $\gamma_c \sim 3\alpha/2$ as $\epsilon \to 0$. At finite ϵ, the localized states for A that were computed in [**26**] are wave-packet type solutions consisting of closely spaced pulses. In the singular limit $\epsilon \to 0$, and with $\alpha < \gamma < \gamma_c \sim 3\alpha/2$, these wave-packet localized solutions were found in [**26**] to lead to a pattern of well-separated hotspots. An asymptotic analysis, based on geometric singular perturbation theory, was given in [**26**] for the construction of a solitary hotspot solution on the infinite line when $\alpha < \gamma < 3\alpha/2$. However, as remarked in [**26**], there were some issues in the asymptotic matching procedure in this construction that were left unresolved. Homoclinic snaking behavior has been well-studied in other systems, such as the Swift-Hohenberg model (see [**3**] and the references therein). Moreover, it has been shown recently in [**4**] that homoclinic snaking behavior is a rather generic feature of solutions to certain types of RD systems near a subcritical Turing bifurcation point.

In contrast to [**26**], our study of hotspot equilibria and dynamics in the singular limit $\epsilon \to 0$ will focus on the finite domain problem for the regime $\gamma > 3\alpha/2$, for which the spatially homogeneous steady-state is linearly unstable. In our analysis of (1.1) it is convenient to introduce the new variable V, as first introduced in [**21**], defined by

$$V \equiv \rho/A^2 \,. \tag{1.3}$$

In terms of A and V, (1.1) transforms to the PDE system

$$A_t = \epsilon^2 A_{xx} - A + VA^3 + \alpha \,, \qquad \left(A^2 V\right)_t = D\left(A^2 V_x\right)_x - VA^3 + \gamma - \alpha \,, \tag{1.4}$$

on $-\ell < x < \ell$, with $A_x = V_x = 0$ at $x = \pm\ell$. The corresponding steady-state problem for (1.4) is

$$\epsilon^2 A_{xx} - A + VA^3 + \alpha = 0 \,, \qquad D\left(A^2 V_x\right)_x - VA^3 + \gamma - \alpha = 0 \,. \tag{1.5}$$

We use the method of matched asymptotic expansions, together with the numerical bifurcation software `AUTO-07p` to analyze the bifurcation properties of steady-state hotspot solutions of (1.5) in the limit $\epsilon \to 0$ for the regime $D = \mathcal{O}(1)$ when $\gamma > 3\alpha/2$. It will be shown, both analytically and numerically, that new hotspots of criminal activity can be nucleated at the domain boundary or in the middle of two adjacent hotspots, and that such events are characterized by a saddle-node bifurcation point of the corresponding bifurcation diagram. We refer to such nucleations as "peak

insertion" events, and they occur whenever the distance between neighboring hotspots, or between a hotspot and the domain boundary, increases beyond a critical threshold. This "peak insertion" behavior effectively determines the minimum number of steady-state hotspots that will occur for a given domain length. Furthermore, we show that the peak insertion behavior for (1.5) is very similar to the mechanism characterizing the onset of the rupture, and ultimate self-replication, of mesa patterns in RD systems (cf. [**20**]), and the breakup of droplets for a diffusive interface surface tension model under compressible flow (cf. [**25**]).

Our leading-order-in-ϵ asymptotic theory for the construction of steady-state hotspot solutions is found to agree well with full numerical results for (1.5) only when ϵ is very small. A more refined asymptotic theory, based on a detailed analysis of a triple-deck structure near the core of the hotspot and the retention of a certain switchback term that is logarithmic in ϵ, is shown to provide a significantly better approximation of hotspot equilibria at moderately small values of ϵ. Switchback terms also arise in the singular perturbation analysis of some other problems, including model problems of low Reynolds number flows (cf. [**22**], [**23**], [**29**]), and the analysis in [**24**] of singular solutions to a PDE model for the deflection of a micro-plate capacitor. In order to include the effect of switchback correction terms, we use a novel procedure, somewhat similar to the renormalization approach in [**7**], whereby the leading-order-in-ϵ asymptotic theory can still be used upon re-defining a certain term with an ϵ-dependent quantity.

Through the derivation and analysis of a nonlocal eigenvalue problem, we show that the multi-hotspot steady-state solutions are unconditionally linearly stable on an $\mathcal{O}(1)$ time-scale when $D = \mathcal{O}(1)$, regardless of the number of hotspots and the value of D. The previous study [**21**] of the stability of hotspot equilibria for the regime $D = \mathcal{O}(\epsilon^{-2})$ showed that K-hotspot equilibria with $K \geq 2$ are linearly stable on an $\mathcal{O}(1)$ time-scale only when $D < D_{0K}/\epsilon^{-2}$ for some constant D_{0K}. For other RD activator-inhibitor systems, without the chemotactic term, nonlocal eigenvalue problems characterizing the stability of multi-spike patterns in 1-D on $\mathcal{O}(1)$ time-scales have been derived and analyzed in [**10**], [**15**], [**18**], [**36**], [**37**], [**38**] (see also the references therein).

The refined asymptotic theory for the construction of hotspot equilibria is shown to be central for deriving a differential algebraic system (DAE) characterizing the slow dynamics of a collection of quasi-steady hotspots for the time-dependent problem (1.4). From this DAE system, it is shown that the dynamic interactions between neighbouring hotspots are repulsive. Therefore, due to the geometrical constraint of the 1-D domain, peak insertion events that are triggered dynamically as a result of the distance between two neighbouring hotspots exceeding some critical threshold are not typically possible in 1-D. This behavior is qualitatively different than the merging-emerging dynamics of localized peaks for the chemotaxis-growth model of [**27**], whereby localized peaks experience attractive, rather than repulsive, dynamics. Peak insertion events, together with attractive dynamics between neighboring peaks, was shown in [**27**] to lead to spatio-temporal chaotic behavior of localized peaks for the chemotaxis-growth model.

We emphasize that our DAE system for the evolution of a single hotspot for the urban crime model (1.4) has a rather different form to that for the dynamics of a single localized spike for other singularly perturbed RD systems such as the Gierer-Meinhardt, Schnakenberg, and Gray-Scott systems, studied in [**6**], [**11**], [**12**], [**14**], [**30**], [**35**] (see also the references therein). In these previous studies, the outer problem away from a spike is linear and its solution for the inhibitor variable can be represented in terms of a Green's function. This leads to a single, explicit, ODE for the evolution of a spike. In contrast, in our analysis of (1.4), the outer problem is nonlinear and there is an intricate triple-deck inner layer structure near the hotspot core for the slow V variable that must be resolved. The resolution of this intricate inner layer structure leads to the generation of switchback terms characterizing the correction terms for the outer expansion away from the core of the hotspot. Overall, this analysis leads to a DAE system rather than a single ODE characterizing the slow motion of a single hotspot.

The outline of the paper is as follows. In §2, we provide a leading-order construction of a single hotspot steady-state solution in the limit $\epsilon \to 0$ for $D = \mathcal{O}(1)$. By reflecting and gluing this single hotspot solution, equilibria with multiple hotspots are obtained. In §3 we show that steady-state patterns with K interior hotspots are linearly stable on an $\mathcal{O}(1)$ time-scale. In §4 we present numerical bifurcation results for hotspot equilibria computed using the bifurcation software `AUTO-07p` (cf. [**9**]). These results show a saddle-node bifurcation structure of hotspot equilibria and a peak insertion behavior near the saddle-node bifurcation point. In §5 we present a higher-order asymptotic theory to construct a steady-state hotspot solution, and in §5.1 we study analytically the onset of peak insertion behavior near the saddle-node bifurcation point. In §6 we derive a differential-algebraic system of ODE's characterizing the slow dynamics of a collection of hotspots for (1.4). Finally, in §7, we briefly discuss a few open problems that warrant further study.

2 The Steady-State Hotspot Solution: Leading-Order Theory

In this section we use the method of matched asymptotic expansions in the limit $\epsilon \to 0$ to construct a leading-order approximation of a steady-state solution with a single hotspot, or spike, for (1.5) on a domain of length 2ℓ. For a fixed D, we will show that such a solution exists only if ℓ is below a threshold. The hotspot solution for (1.5) is an even solution with a spike centered at the midpoint of the interval $-\ell < x < \ell$, and that satisfies $A_x = V_x = 0$ at $x = \pm l$. By reflecting and gluing copies of this single hotspot solution, we can readily obtain a K-hotspot solution on the larger interval $-S < x < S$, with $S = K\ell$. The key difference between our analysis and that in [**21**] is that here we consider the $D = \mathcal{O}(1)$ regime, which leads below to a nonlinear ODE characterizing the outer solution. In [**21**], the limit $D \gg \mathcal{O}(1)$ was considered, which leads to a linear outer problem and, consequently, a more elementary construction of the hotspot solution than for the case $D = \mathcal{O}(1)$.

As in [**21**], a hotspot is characterized by a localized region of width $\mathcal{O}(\epsilon)$ near $x = 0$ where $A \gg 1$ and $V \ll 1$. In the outer region, where $|x| \gg \mathcal{O}(\epsilon)$, we have from (1.5) that both A and V are $\mathcal{O}(1)$ when $D = \mathcal{O}(1)$.

To determine the scalings for the inner region, we introduce the inner variable $y = \epsilon^{-1}x$ so that (1.5) becomes

$$A_{yy} - A + VA^3 - \alpha = 0\,, \qquad D\epsilon^{-2}\left(A^2V_y\right)_y - VA^3 + \gamma - \alpha = 0\,. \tag{2.1}$$

In this inner region, we pose $A = \mathcal{O}(\epsilon^{-p})$, with $p > 0$, and $V = \mathcal{O}(\epsilon^q)$. In order to obtain a homoclinic solution solution characterizing the hotspot core, we must balance $\mathcal{O}(A) = \mathcal{O}(VA^3)$ in the first equation of (2.1), which yields $q = 2p$. To determine the second scaling relation, we integrate the second equation in (1.5) over $|x| \le \ell$ to obtain that $\int_{-\ell}^{\ell} VA^3\,dx = \mathcal{O}(1)$. In order that the inner region makes an $\mathcal{O}(1)$ contribution to this integral, we require that $1 + q - 3p = 0$. With $q = 2p$, this yields that $p = 1$ and $q = 2$.

One of the key differences between the analysis for our $D = \mathcal{O}(1)$ regime and that in [**21**] for $D \gg \mathcal{O}(1)$, is that here V is characterized by a rapid transition of scale from $V = \mathcal{O}(\epsilon^2)$ in the inner region to $V = \mathcal{O}(1)$ in the outer region. In the analysis of [**21**] for the $D \gg 1$ case, it was found that $V \ll 1$ *uniformly* across $-\ell < x < \ell$. A detailed analysis of this rapid transition of scale for V, which requires introducing an intermediate layer between the inner and outer scales, is essential for characterizing the slow dynamics of a collection of hotspots. This more refined analysis is given below in §5. In the remainder of this section we only construct a leading-order hotspot solution.

The simple scaling analysis above motivates the following inner expansion for (2.1):

$$A \sim \epsilon^{-1}A_0 + A_1 + \dots\,, \qquad V \sim \epsilon^2 V_0 + \epsilon^3 V_1 + \dots\,.$$

Upon substituting this expansion into (2.1) we obtain that V_0 is a constant independent of y and that A_0 satisfies $A_{0yy} - A_0 + V_0A_0^3 = 0$. This yields that

$$A_0 = \frac{w(y)}{\sqrt{V_0}}\,, \tag{2.2}$$

where $w(y) = \sqrt{2}\,\mathrm{sech}\, y$ is the unique homoclinic solution to

$$w_{yy} - w + w^3 = 0\,, \quad -\infty < y < \infty\,; \qquad w(0) > 0\,, \quad w_y(0) = 0\,, \quad w \to 0 \quad \text{as} \quad y \to \pm\infty\,. \tag{2.3}$$

To determine V_0, we first need to construct an outer solution on the intervals $0^+ < x < \ell$ and $-\ell < x < 0^-$. Since the hotspot solution is even, we need only consider the range $0^+ < x < \ell$. On this range, we expand $A \sim a_0 + o(1)$ and $V \sim v_0 + o(1)$. Upon substituting this expansion into (1.5) we obtain

$$D\left(a_0^2 v_{0x}\right)_x - v_0 a_0^3 + \gamma - \alpha = 0\,, \qquad v_0 = g(a_0) \equiv \frac{(a_0 - \alpha)}{a_0^3}\,. \tag{2.4}$$

In order that v_0 can match to the inner solution, we require that $v_0(0^+) = 0$, so that $a_0(0^+) = \alpha$. Then, upon combining the two equations in (2.4), it follows that in the outer region a_0 satisfies the nonlinear BVP

$$D\left(f(a_0)a_{0x}\right)_x = a_0 - \gamma\,, \qquad 0^+ < x < \ell\,; \qquad a_0(0^+) = \alpha\,, \quad a_{0x}(\ell) = 0\,, \tag{2.5}$$

where we have defined $f(a_0)$ by

$$f(a_0) \equiv \frac{(3\alpha - 2a_0)}{a_0^2} = a_0^2 g'(a_0)\,. \tag{2.6}$$

For the well-posedness of this outer problem (2.5) we require that $f(a_0)$ is non-vanishing on $0^+ < x < \ell$. Since the only zero of $f(a_0)$ is at $3\alpha/2$ and $f(\alpha) = \alpha^{-1} > 0$, we shall consider the range $\alpha < a_0 < 3\alpha/2$. By our previous

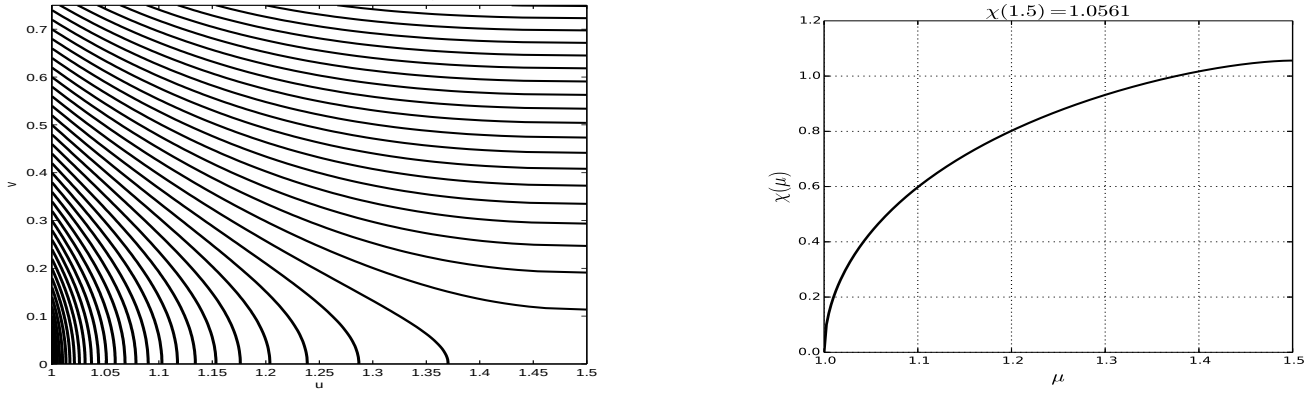

(a) (b)

Figure 3. (a) Phase portraits of (2.7) with trajectories emanating from the line $u(0) = \alpha$. Only if $v(0)$ is below a threshold will v hit zero at some finite "time" $x = \ell$. (b) The function $\chi(\mu)$, from (2.11), that determines the outer solution for any $\mu \equiv a_0(\ell)$ on $\alpha < \mu < 3\alpha/2$. In both figures, the parameter values are $D = 1$, $\gamma = 2$, $\alpha = 1$.

assumption that $\gamma > 3\alpha/2$, which implies that we are in the Turing-unstable regime, it follows that the right-hand side of the differential equation in (2.5) is always negative on the range $\alpha < a_0 < 3\alpha/2$. This yields that $a_{0x} > 0$ on $0^+ < x < \ell$ when $\alpha < a_0 < 3\alpha/2$.

Before reducing (2.5) to a quadrature, we first qualitatively illustrate these results concerning the leading-order outer solution by using an elementary phase plane analysis. To do so, we introduce the temporary notation $u \equiv a_0$ and $v \equiv f(a_0)a_{0x} = f(u)u'$ to rewrite (2.5) in the following usual form of a dynamical system:

$$u' = \frac{v}{f(u)}\,, \qquad v' = \frac{(u-\gamma)}{D}\,. \tag{2.7}$$

We seek to identify trajectories in the u, v phase-plane that satisfy $u(0) = \alpha$ and $v(\ell) = 0$, corresponding to the boundary conditions of (2.5). From the phase-plane shown in Fig. 3(a), we clearly observe two types of trajectories and a critical threshold v_c for $v(0)$. If $v(0) < v_c$, then the trajectory converges to $v(\ell) = 0$ for some finite positive ℓ. However, if $v(0) > v_c$, then the solution develops a singularity as $u \to \left(\frac{3\alpha}{2}\right)^-$ where $u' \to +\infty$. Near where this singularity occurs a new local boundary layer near $x = \ell$ must be constructed. As motivated by the numerical bifurcation results in §4, in §5.1 we analytically show that this singularity behavior is associated with a fold-point bifurcation of equilibrium hotspot solutions, and it characterizes the onset of a hotspot insertion phenomena at $x = \ell$.

We now reduce the BVP (2.5) to a simple quadrature. We first multiply (2.5) by $f(a_0)a_{0x}$ and integrate the resulting expression using $a_{0x}(\ell) = 0$ to get

$$\frac{D}{2}\left(f(a_0)a_{0x}\right)^2 = \int_\ell^x f(a_0)(a_0-\gamma)\frac{da_0}{d\eta}\,d\eta\,.$$

Since $a_{0x} > 0$, we have upon labelling $\mu \equiv a_0(\ell)$ that

$$\frac{D}{2}\left(f(a_0)a_{0x}\right)^2 = \int_\mu^{a_0} f(w)(w-\gamma)\,dw = G(\mu) - G(a_0)\,, \tag{2.8 a}$$

where $G(u)$, satisfying $G'(u) = f(u)(\gamma - u)$, is given explicitly by

$$G(u) \equiv 2u - (2\gamma + 3\alpha)\log u - \frac{3\alpha\gamma}{u}\,. \tag{2.8 b}$$

Notice that $G(u)$ is a monotone increasing function on $\alpha < u < 3\alpha/2$ when $\gamma > 3\alpha/2$.

Next, we take the appropriate square root in (2.8 a) and integrate again using $a_0(0) = \alpha$ to obtain

$$\sqrt{\frac{2}{D}}x = \int_\alpha^{a_0} \frac{f(w)\,dw}{\sqrt{G(\mu) - G(w)}}\,. \tag{2.9}$$

Finally, upon setting $x = \ell$ and $a_0(\ell) = \mu$, we obtain an implicit equation for μ given by

$$\sqrt{\frac{2}{D}}\ell = \chi(\mu)\,, \qquad \chi(\mu) \equiv \int_{\alpha}^{\mu} \frac{f(w)\,dw}{\sqrt{G(\mu) - G(w)}}\,. \tag{2.10}$$

To show that the function $\chi(\mu)$ is well-defined, we show that the improper integral is convergent by using $f(u) = G'(u)/(\gamma - u)$ together with integration by parts to derive

$$\chi(\mu) = \int_{\alpha}^{\mu} \frac{G'(w)\,dw}{(\gamma - w)\sqrt{G(\mu) - G(w)}} = \frac{2\sqrt{G(\mu) - G(\alpha)}}{\gamma - \alpha} + 2\int_{\alpha}^{\mu} \frac{\sqrt{G(\mu) - G(w)}}{(\gamma - w)^2}\,dw\,. \tag{2.11}$$

This last expression shows that $\chi(\mu)$ is a well-defined, positive and increasing function on the closed interval $\alpha \le u \le 3\alpha/2$ when $\gamma > 3\alpha/2$. In Fig. 3(b) we plot $\chi(\mu)$ on this range when $\alpha = 1$ and $\gamma = 2$.

For a solution $a_0(x)$ to (2.5) to exist, then $\mu = a_0(\ell)$ on $\alpha \le \mu \le 3\alpha/2$ must satisfy the implicit equation

$$\chi(\mu) = \sqrt{\frac{2}{D}}\ell\,. \tag{2.12}$$

Notice that the left-hand side of this expression depends on γ and α, appearing implicitly through $\chi(\mu)$, while the right-hand side depends on the ratio $\ell/\sqrt{D}$. To highlight the significance of (2.12), we first recall that $\alpha \le a_0(x) \le \mu = a_0(\ell) \le 3\alpha/2 < \gamma$, so that the largest possible value of μ is $3\alpha/2$. For $\gamma = 2$ and $\alpha = 1$, we calculate numerically from (2.11) (see Fig. 3(b)) that

$$\chi_{\max} \equiv \chi\left(\frac{3\alpha}{2}\right) \approx 1.0561\,. \tag{2.13}$$

For a fixed D, we can use $\chi_{\max}$ to characterize the maximum length $\ell_{\max}$ for which the outer solution exists as

$$\ell_{\max} = \sqrt{\frac{D}{2}}\chi_{\max}\,. \tag{2.14}$$

Since $\chi(\mu)$ is monotonic, we can invert the one-to-one function $\chi(\mu)$ to compute $a_0(\ell) = \mu = \chi^{-1}(\sqrt{\frac{2}{D}}\ell)$ for any $\ell \in (0, \ell_{\max}]$. In this way, we identify $v_0(\ell) = g\left(a_0(\ell)\right)$ from (2.4).

Since χ^{-1}, like χ, is strictly monotonic, this implies that, unlike the regime in [**21**] where $D \gg \mathcal{O}(1)$, the interval length of any adjacent outer regions for a multiple hotspot solution must coincide. Therefore, an asymmetric steady-state multi-hotspot pattern, characterized by hotspots of different heights, is impossible in the $D = \mathcal{O}(1)$ regime.

Correspondingly, if we fix ℓ, we can then use $\chi_{\max}$ to characterize the minimum value $D_{\rm crit}$ of D for which the outer solution exists as

$$D_{\rm crit} \equiv \frac{2\ell^2}{\chi_{\max}^2}\,. \tag{2.15}$$

In most of our numerical simulations below, we consider the domain $(-1, 1)$ containing K interior hot-spots. To determine the minimum value of D for this pattern, we simply put $\ell = 1/K$ to obtain the critical thresholds

$$D_{{\rm crit},K} = \frac{2}{K^2\chi_{\max}^2}\,. \tag{2.16}$$

To compare with our full numerical results in §4, we calculate for $\alpha = 1$ and $\gamma = 2$ that

$$D_{{\rm crit},1} \approx 1.7930\,, \qquad D_{{\rm crit},2} \approx 0.4483\,, \qquad D_{{\rm crit},4} \approx 0.1121\,. \tag{2.17}$$

To complete the leading-order theory, we must determine the leading-order constant V_0 in the inner expansion. By using the outer expansion, we obtain the following limiting behavior from (2.4) and (2.9):

$$A \sim a_0(0^+) = \alpha\,, \qquad v_{0x}(0^+) \sim g'(\alpha)a_{0x}(0^+) = \frac{1}{\alpha^2}\sqrt{\frac{2}{D}}\sqrt{G(\mu) - G(\alpha)}\,. \tag{2.18}$$

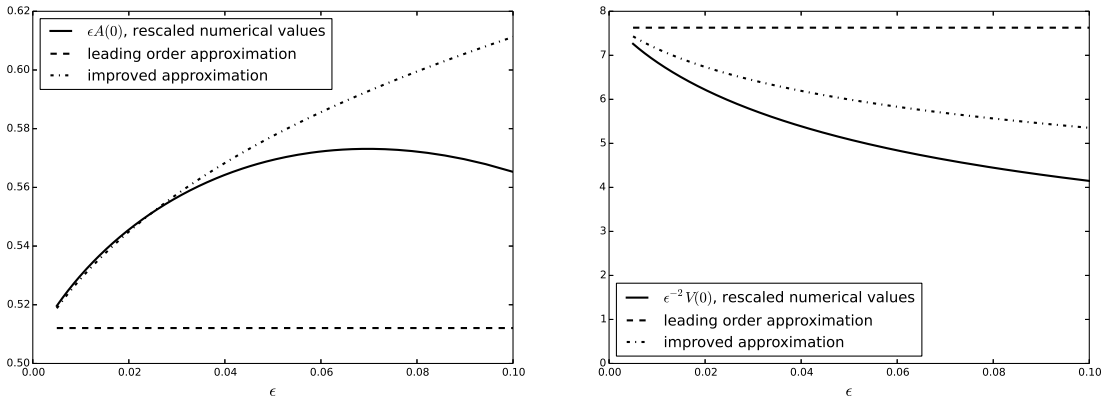

Figure 4. Comparison of numerical and asymptotic results for $\epsilon A(0)$ (left panel) and for $\epsilon^{-2}V(0)$ (right panel) as ϵ is decreased for a single hotspot centered at the origin. The parameter values are $\alpha = 1$, $\gamma = 2$, $\ell = 1$, and $D = 2$. The dashed horizontal lines are the leading-order prediction of $\epsilon A(0) \approx \sqrt{2}/\sqrt{V_0}$ and $\epsilon^{-2}V(0) \approx V_0$, where V_0 is given in (2.21). The thin dotted curves are from the improved asymptotic theory with V_0 now given by (5.27).

To determine V_0, we integrate the V-equation of (1.5) over an intermediate region $(-\delta, \delta)$, with $\epsilon \ll \delta \ll 1$, to obtain

$$D\left(A^2 V_x\right)\big|_{x=-\delta}^{x=\delta} = \int_{-\delta}^{\delta} V A^3\, dx + \mathcal{O}(\delta)\,. \tag{2.19}$$

Since $\delta \gg \epsilon$, the outer expansion (2.18) is used to evaluate the left-hand side of (2.19), upon noting the symmetry condition $v_{0x}(0^+) = -v_{0x}(0^-)$. In contrast, since $VA^3 = O(\epsilon^{-1})$ in the inner region, the integral in (2.19) is dominated by contributions from the inner region where $A \sim w/\sqrt{V_0}$ and $V \sim \epsilon^2 V_0$. In this way, using $\delta \gg \epsilon$ and $w(y) = \sqrt{2}\,\mathrm{sech}\, y$, we calculate that

$$D\alpha^2\left(v_{0x}(0^+) - v_{0x}(0^-)\right) = 2D\alpha^2 v_{0x}(0^+) \sim \frac{1}{\sqrt{V_0}} \int_{-\infty}^{\infty} w^3\, dy = \frac{\sqrt{2}\pi}{\sqrt{V_0}}\,. \tag{2.20}$$

Finally, upon using (2.18) for $v_{0x}(0^+)$, we obtain

$$V_0 = \frac{\pi^2}{4D}\left[G(\mu) - G(\alpha)\right]^{-1}\,. \tag{2.21}$$

Here $\mu = a_0(\ell)$ is a root of (2.12) and $G(u)$ is defined in (2.8 *b*).

As ϵ is decreased, and for $\alpha = 1$, $\gamma = 2$ and $D = 2$, in Fig. 4 we compare our leading-order asymptotic results for $\epsilon A(0)$ (left panel) and for $\epsilon^{-2}V(0)$ (right panel) with corresponding full numerical results computed from (1.5) using the continuation software `AUTO-07p` (cf. [**9**]). The leading-order asymptotic results are $\epsilon A(0) \sim \sqrt{2}/\sqrt{V_0}$ and $\epsilon^{-2}V(0) \sim V_0$, where V_0 is defined in (2.21). These comparisons show that the leading-order asymptotic theory only agrees well with the full numerical results when ϵ is very small. As such, in order to obtain decent agreement between the asymptotic theory and full numerical results when ϵ is only moderately small, we must provide a higher-order asymptotic theory. This more refined asymptotic theory, done in §5, shows that the error in the leading-order prediction is in fact $\mathcal{O}(-\epsilon \log \epsilon)$, which explains why the leading-order theory is rather inaccurate unless ϵ is very small. The asymptotic results from this improved theory are shown by the thin dotted curves in Fig. 4.

3 NLEP Stability Analysis

In this section we analyze the stability of steady-state hotspot solutions to (1.4) in the regime where $D = \mathcal{O}(1)$. We show that all eigenvalues λ, with $\lambda = \mathcal{O}(1)$, of the linearization satisfy $\mathrm{Re}(\lambda) < 0$ so that steady-state hotspot solutions are stable on an $\mathcal{O}(1)$ time-scale.

We let $a_e(x)$, $v_e(x)$ be a hotspot solution to the steady-state problem (1.5). Recall that in the inner region near the

core of the hotpsot, we have $a_e = \mathcal{O}(\epsilon^{-1})$ and $v_e = \mathcal{O}(\epsilon^2)$, while both a_e and v_e are $\mathcal{O}(1)$ in the outer region. Upon introducing the perturbation

$$A = a_e + e^{\lambda t}\phi\,, \qquad V = v_e + e^{\lambda t}\epsilon^3\psi\,,$$

into (1.4), we obtain the following singularly perturbed eigenvalue problem on $|x| < \ell$:

$$\epsilon^2\phi_{xx} - \phi + 3v_e a_e^2\phi + \epsilon^3 a_e^3\psi = \lambda\phi\,, \tag{3.1 a}$$

$$D\left(a_e^2\epsilon^3\psi_x + 2a_e v_{ex}\phi\right)_x = 3a_e^2 v_e\phi + \epsilon^3 a_e^3\psi + \lambda\left(\epsilon^3 a_e^2\psi + 2a_e v_e\phi\right)\,. \tag{3.1 b}$$

We remark that our choice of $\mathcal{O}(1)$ and $\mathcal{O}(\epsilon^3)$ perturbations for A and V produce a distinguished balance for all terms in the equation for ϕ in the inner region, where the length scale is $\mathcal{O}(\epsilon)$.

To examine the stability of a single hotspot solution or a multiple hotspot solution we impose either homogeneous Neumann or Floquet-type boundary conditions, respectively, on $x = \pm\ell$, as was done in [**21**]. However, as we show below, in the regime $\epsilon \ll 1$ and $D = \mathcal{O}(1)$, the leading-order stability problem is independent of the specific choice of boundary condition, and this leading-order problem predicts that hotspot equilibria are unconditionally linearly stable to $\mathcal{O}(1)$ time-scale perturbations.

We begin by deriving the leading-order stability problem for a hotspot solution centered at the origin in the domain $|x| \le \ell$. The eigenfunction component ϕ is singularly perturbed. It has rapid spatial variation near $x = 0$, but varies on an $\mathcal{O}(1)$ scale away from the hotspot core. The leading-order stability problem will consist of a nonlocal eigenvalue problem (NLEP) for ϕ on the inner-scale centered at $x = 0$. Alternatively, the eigenfunction component ψ is not singularly perturbed and varies on an $\mathcal{O}(1)$ scale across the entire domain $|x| \le \ell$.

In the inner region near the core of the hotspot at $x = 0$ we introduce the local variables $y = x/\epsilon$, $\phi = \Phi(y)$, and $\psi = \Psi(y)$. Then, from (3.1 *b*), we observe that the leading-order equation is $\left(w^2\Psi_y\right)_y = 0$. The bounded solution to this equation is the constant solution $\Psi = \psi(0)$, which must be determined in the ensuing analysis. With regards to Φ, we recall from §2 that $a_e \sim \epsilon^{-1}w/\sqrt{V_0}$ and $v_e \sim \epsilon^2 V_0$. Upon substituting these expressions into (3.1 *a*), we obtain the leading-order inner problem for $\Phi(y)$ on $-\infty < y < \infty$, given by

$$L_0\Phi + \frac{1}{V_0^{3/2}}w^3\psi(0) = \lambda\Phi\,, \qquad L_0\Phi \equiv \Phi_{yy} - \Phi + 3w^2\Phi\,, \tag{3.2}$$

where $\Phi \to 0$ as $|y| \to \infty$.

Next, we integrate (3.1 *b*) over $-\delta < x < \delta$ to derive a "jump condition" for ψ, valid as $\epsilon \to 0$. Here, δ is any intermediate scale, satisfying $\epsilon \ll \delta \ll 1$. This integration yields

$$\epsilon^3 D\left[a_e^2\psi_x\right]_0 + 2D\left[a_e v_{ex}\phi\right]_0 \sim 3\epsilon\int_{-\delta/\epsilon}^{\delta/\epsilon} w^2\Phi\,dy + \frac{\epsilon\psi(0)}{V_0^{3/2}}\int_{-\delta/\epsilon}^{\delta/\epsilon} w^3\,dy$$
$$+\lambda\left[2\epsilon^2\sqrt{V_0}\int_{-\delta/\epsilon}^{\delta/\epsilon} w\Phi\,dy + \frac{\epsilon^2\psi(0)}{V_0}\int_{-\delta/\epsilon}^{\delta/\epsilon} w^2\,dy\right]\,.$$

Here we have defined $[h]_0 \equiv \lim_{x\to 0^+} h(x) - \lim_{x\to 0^-} h(x)$. For $\epsilon \to 0$, we can then neglect the terms in the square brackets in the expression above, let $\delta/\epsilon \to +\infty$, and use $a_e \sim \alpha$ as $x \to 0^\pm$ from the outer solution. In this way, we obtain the following asymptotic approximation of the jump condition:

$$\epsilon^3 D\alpha^2\left[\psi_x\right]_0 + 2D\alpha\left[v_{ex}\phi\right]_0 \sim 3\epsilon\int_{-\infty}^{\infty} w^2\Phi\,dy + \frac{\epsilon\psi(0)}{V_0^{3/2}}\int_{-\infty}^{\infty} w^3\,dy\,. \tag{3.3}$$

Next, we examine the outer expansion for ϕ and ψ in order to estimate the left-hand side of (3.3). From the outer approximation of (3.1 *a*), we use $v_\epsilon \sim v_0$ and $a_\epsilon \sim a_0$ to obtain that

$$\left(3v_0 a_0^2 - 1\right)\phi + \epsilon^3 a_0^3\psi \sim \lambda\phi\,.$$

Then, since $v_0 = g(a_0)$, where $g(a_0)$ is defined in (2.4), we solve for ϕ_0 to obtain

$$\phi = \epsilon^3\tilde{\phi}\,, \qquad \tilde{\phi} \equiv \left(\frac{a_0^3}{\lambda - 2 + 3\alpha/a_0}\right)\psi\,. \tag{3.4}$$

Since $\alpha \le a_0 < 3\alpha/2$ for $|x| \le \ell$, we conclude by examining the denominator in (3.4) that $\tilde{\phi}$ is analytic in $\mathrm{Re}(\lambda) \ge 0$. We then let $x \to 0^{\pm}$ in (3.4) to get

$$\phi(0^{\pm}) = \epsilon^3 \left(\frac{\alpha^3}{\lambda + 1} \right) \psi(0) \,. \tag{3.5}$$

We then use (3.5), together with $v_{ex}(0^{\pm}) \sim g'(\alpha) a_{0x}(0^{\pm})$ and $g'(\alpha) = 1/\alpha^3$, to estimate the second term on the left-hand side of (3.3) as

$$2D\alpha \left[v_{ex} \phi \right]_0 \sim \left(\frac{2D\alpha}{\lambda + 1} \right) \epsilon^3 \psi(0) \left[a_{0x} \right]_0 \,.$$

In this way, we obtain that the asymptotic jump condition (3.3) for $\psi(x)$ becomes

$$\epsilon^2 D \left(\alpha^2 \left[\psi_x \right]_0 + \frac{2\alpha}{\lambda + 1} \psi(0) \left[a_{0x} \right]_0 \right) \sim 3 \int_{-\infty}^{\infty} w^2 \Phi \, dy + \frac{\psi(0)}{V_0^{3/2}} \int_{-\infty}^{\infty} w^3 \, dy \,, \tag{3.6}$$

where $a_0(x)$ satisfies the nonlinear BVP (2.5) in the outer region.

Next, we derive the outer problem for $\psi(x)$ on $-\ell < x < 0^-$ and on $0^+ < x < \ell$ by considering the outer limit for (3.1 *b*), where we have $a_\epsilon \sim a_0$, $v_\epsilon \sim v_0$, and $\phi \sim \epsilon^3 \tilde{\phi}$. This outer problem is

$$D \left(a_0^2 \psi_x + 2 a_0 v_{0x} \tilde{\phi} \right)_x = 3 a_0^2 v_0 \tilde{\phi} + a_0^3 \psi + \lambda \left(2 a_0 v_0 \tilde{\phi} + a_0^2 \psi \right) \,, \tag{3.7}$$

where $\tilde{\phi}$ depends linearly on ψ from (3.4). We then substitute (3.4), $v_0 = g(a_0)$, and $v_{0x} = g'(a_0) a_{0x}$ into (3.7), where $g(a_0)$ is defined in (2.4). After some algebra, we obtain that (3.7) reduces on $0 < |x| < \ell$ to

$$\left(a_0^2 \psi_x + \left(\frac{3\alpha - 2a_0}{3\alpha + a_0(\lambda - 2)} \right) \left(a_0^2 \right)_x \psi \right)_x = \left(\frac{(\lambda + 1) a_0^3 + \lambda a_0 (\alpha + a_0 \lambda)}{\lambda - 2 + 3\alpha / a_0} \right) \psi \,. \tag{3.8}$$

The problem for ψ is to solve (3.8) on the intervals $0 < x < \ell$ and $-\ell < x < 0$, together with the continuity of ψ across $x = 0$, the jump condition (3.6), and subject to either homogeneous Neumann or Floquet-type boundary conditions imposed at $x = \pm \ell$ depending on whether we are considering single or multiple hotspot solutions, respectively. From the solution to this problem we can determine $\psi(0)$, which is needed for the inner problem (3.2).

The differential equation (3.8) can be written in the general form

$$\left(b(x) \psi_x + b_1(x, \lambda) \psi \right)_x = b_2(x, \lambda) \psi \,. \tag{3.9}$$

where $b(x) > 0$ on $0 < |x| \le \ell$. Since $\alpha \le a_0 < 3\alpha/2$ for $|x| \le \ell$, we conclude from (3.8) that $b_1(x, \lambda)$ and $b_2(x, \lambda)$ are analytic in $\mathrm{Re}(\lambda) \ge 0$. Since ψ satisfies a linear ODE with analytic coefficients in $\mathrm{Re}(\lambda) \ge 0$, any solution to (3.8) must be analytic in $\mathrm{Re}(\lambda) \ge 0$ by classical ODE theory.

Although it is intractable analytically to determine $\psi(x)$ explicitly, we can fortunately determine $\psi(0)$ as $\epsilon \to 0$ simply from the leading-order approximation (3.6) of the jump condition. Since the outer solution satisfying (3.8) is smooth, we have that $\psi_x(0^{\pm})$ is finite and independent of ϵ. Letting $\epsilon \to 0$ in the jump condition (3.6) we identify that

$$\psi(0) \sim -3 V_0^{3/2} \left(\frac{\int_{-\infty}^{\infty} w^2 \Phi \, dy}{\int_{-\infty}^{\infty} w^3 \, dy} \right) \,. \tag{3.10}$$

Finally, upon substituting (3.10) into (3.2), we obtain the nonlocal eigenvalue problem (NLEP)

$$L_0 \Phi - 3 w^3 \left(\frac{\int_{-\infty}^{\infty} w^2 \Phi \, dy}{\int_{-\infty}^{\infty} w^3 \, dy} \right) = \lambda \Phi \,, \quad -\infty < y < \infty \,; \qquad \Phi \to 0 \quad \text{as} \quad |y| \to \infty \,. \tag{3.11}$$

Since this NLEP is independent of the boundary conditions for ψ on $x = \pm \ell$, it applies to both single and multiple hotspot solutions. As shown in Lemma 3.2 of [**21**], the NLEP (3.11) is explicitly solvable in the sense that its discrete spectrum can be found analytically. Lemma 3.2 of [**21**] shows that any nonzero eigenvalue of (3.11) must satisfy $\mathrm{Re}(\lambda) < 0$.

4 Numerical Computations of Hotspot Equilibria: Bifurcation Structure

In this section we show full numerical bifurcation results for hotspot equilibria of (1.5) computed using the continuation software `AUTO-07p` (cf. [**9**]). These computations show that new hotspots are created near the endpoints $x = \pm l$ or at the midpoint between two hotspots when D approaches a saddle-node bifurcation value, which we denote by $D_{\rm fold}$. We call this phenomena *hotspot or spike insertion*. Our numerical results show clearly that the fold-point value $D_{\rm fold}$ tends, as $\epsilon \to 0$, to the critical value $D_{\rm crit}$, as derived from the leading-order asymptotic theory of §2. However, unless ϵ is very small, our results show that the leading-order theory for the critical value of D is quantitatively rather inaccurate. This motivates the need for a higher-order asymptotic theory in §5.

By using `AUTO-07p` we compute from (1.5) the bifurcation diagrams of branches of steady-state solutions starting with either $K = 1$, $K = 2$, or $K = 4$, interior hotspots. Instead of using the L^2 norm, it is more convenient to use the boundary value $A(\ell)$ as the vertical axis on the bifurcation diagram, as this prevents the overlapping of solution branches with boundary hotspots. The horizontal axis on the bifurcation diagram is D. Our computational results for the parameter set $\gamma = 2$, $\alpha = 1$, $\ell = 1$, and $\epsilon = 0.01$, displayed in Fig. 5(a) show that as D is varied, the steady-state solution branch with one interior hotspot is connected to a solution that has an interior hotspot together with a hotspot at each boundary. Boundary hotspots are created at the endpoints $x = \pm\ell$ near the fold point associated with the small norm branch for $A(\ell)$ versus D.

Similar bifurcation results starting from either two or four interior hotspots on the small norm $A(\ell)$ versus D branch are shown in Fig. 5(b) and Fig. 5(c) to be path-connected to solutions with mixed boundary and interior hotspots. We observe that new hotspots are nucleated at the endpoints $x = \pm\ell$ and at the midpoint of the interval between adjacent hotspots at the fold point associated with the small norm solution branch.

In each set of the four solution profiles in Fig. 5 we observe, as expected by symmetry, that the right top and bottom figures have the same value of D at the two fold points where D is smallest. In each case, as we follow the small norm solution branch of $A(\ell)$ versus D towards the fold-point value, we observe a decrease in the amplitude of the hotspot and a gradual bulging up of the solution at the midpoint between hotspots or at the domain boundaries (i.e. at the boundary of the outer regions). This leads to a large amplitude pattern of hotspots when the boundary value $A(\ell)$ exceeds a certain value close to $3\alpha/2 = 1.5$.

As compared to the large $\mathcal{O}(\epsilon^{-1})$ scale of the hotspot amplitude, the nucleation or formation of hotspots near the boundary, or at the midpoint between hotspots, is not so conspicuous in our plots, especially when ϵ is small. However, the implication of hotspot nucleation is interesting qualitatively. It predicts that a new crime hotspot can emerge from an essentially quiescent background state when the parameters are close to a fold-point value in D.

Next, we show how the criminal density changes at the onset of spot insertion. In Fig. 6 we give various plots of $\rho = A^2V$ for values of D at and close to the fold point. We remark that since $\rho = O(1)$ in both the inner and outer regions, i.e. *globally*, the spot insertion phenomenon can be observed quite clearly in these plots.

We now discuss whether the solution branches in Fig. 6 corresponding to parameter values immediately above the fold point, consisting of "small" hotspots between the large amplitude hotspots, are linearly stable or not. An analytical stability theory of the solution branch beyond the fold point would first require an asymptotic construction of such an alternating pattern with new boundary layers for these "small" hotspots (since the previous outer solution is no longer valid), and would be rather intricate to undertake. Although we do not pursue the analysis here, we conjecture that all such patterns are unstable. Indeed, from a number of numerical experiments, we observe that a solution on the "upper" branch evolves quickly to its counterpart directly below on the lower branch, i.e. with the same value of D in the bifurcation diagrams (and all other parameters as well) shown in Fig. 5. In Fig. 7, we show the evolutionary dynamics computed by `PDEPE` using the "upper" branch solutions computed in `AUTO-07p` as initial conditions. In all cases shown, the dynamics stabilizes to exactly the pattern of the solution on the corresponding "lower" branch, with no visible difference.

Our numerical bifurcation results for the fold-point bifurcation along the small norm solution branch for $\gamma = 2$, $\alpha = 1$, $\ell = 1$, and $\epsilon = 0.01$ are

$$D_{\rm fold,1} = 1.5600\,, \qquad D_{\rm fold,2} = 0.3451\,, \qquad D_{\rm fold,4} = 0.0677\,. \tag{4.1}$$

Observe, as expected by symmetry, that these values are quartered as the number of hotspots doubles. However, we observe that the quantitative agreement of these fold-point values with the critical values $D_{{\rm crit},K}$ of (2.17), as computed from the leading-order theory of §2, is suggestive, but is not particularly close even when $\epsilon = 0.01$.

As a result of this rather poor quantitative agreement at finite ϵ, we used `AUTO-07p` (cf. [**9**]) to perform a codimension-two path-following of the fold point as ϵ is decreased. The computations were done for the case of $K = 1$, $K = 2$,

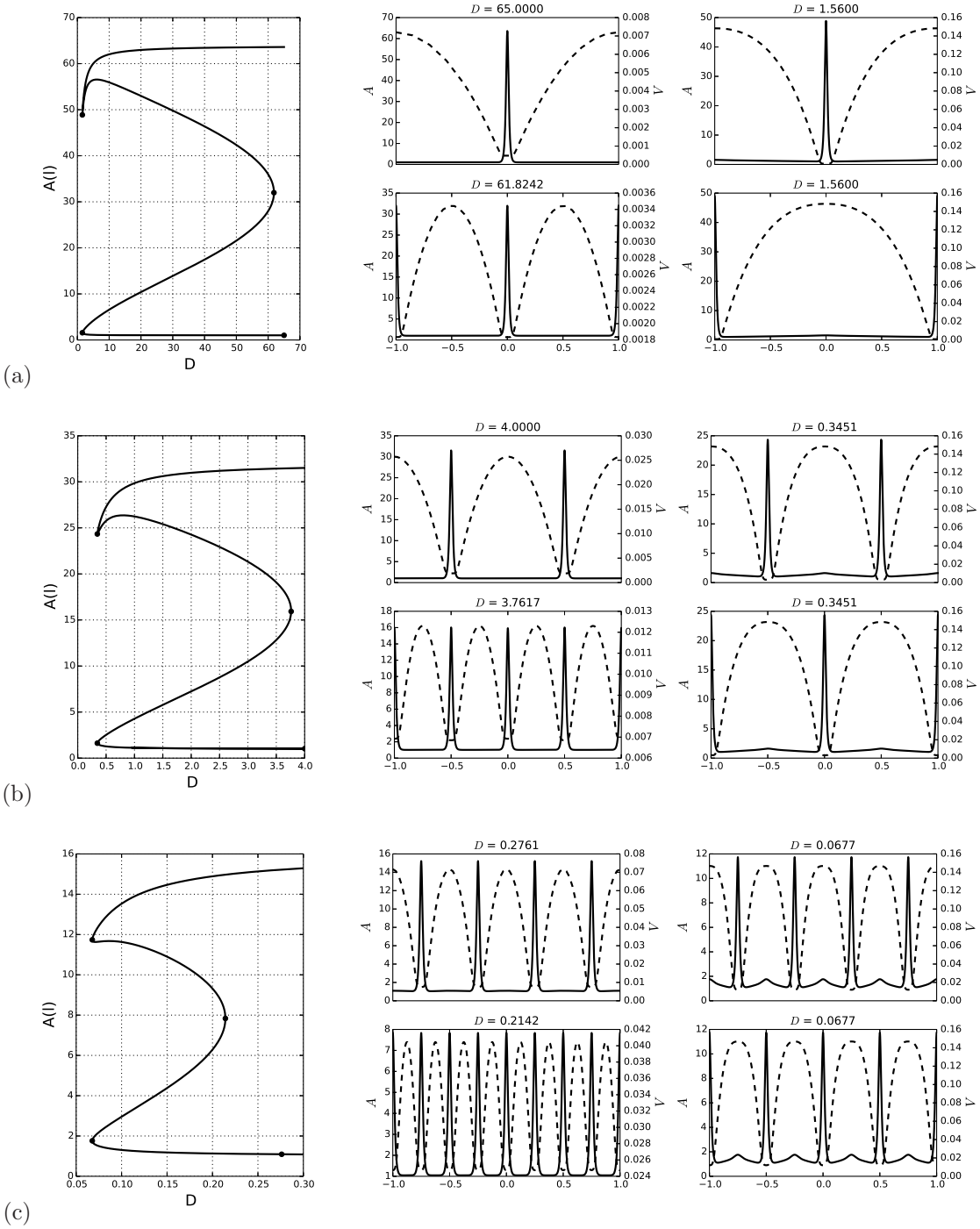

Figure 5. The plots (a), (b) and (c) show the continuation of steady states starting with either one, two, or four, interior hotspots, respectively, for $\epsilon = 0.01$. The other parameters are $\gamma = 2$, $\alpha = 1$, and $\ell = 1$. The solid and dashed curves in the subplots show the profiles of A and V, respectively, at various values of D specified on top of the plots. These values of D correspond to the marked points on the bifurcation diagram as shown on the left. Notice that the range of A and V are on different scales.

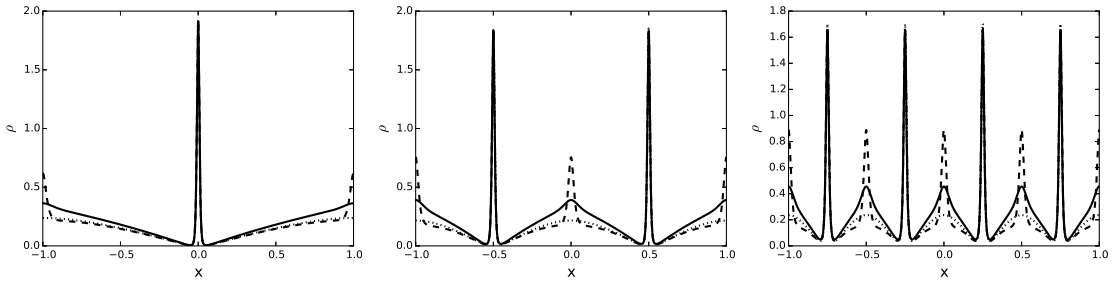

Figure 6. Plots of criminal density ρ near the onset of spot insertion as indicated in Fig. 5. The parameter values are the same, i.e. $\epsilon = 0.01$, $\gamma = 2$, $\alpha = 1$, $\ell = 1$. The solid curves correspond to ρ at the numerically computed fold point, while the dashed curves and dotted curves corresponds to the solutions at some identical values of D close to, but above and below the fold points shown in Fig. 5. Such chosen values of D are 2.0, 0.5 and 0.1 respectively for one, two, or four, interior spikes (before the insertion event), corresponding to the subfigure on the left, center, and right, respectively. The fold point values of D are given in (4.1).

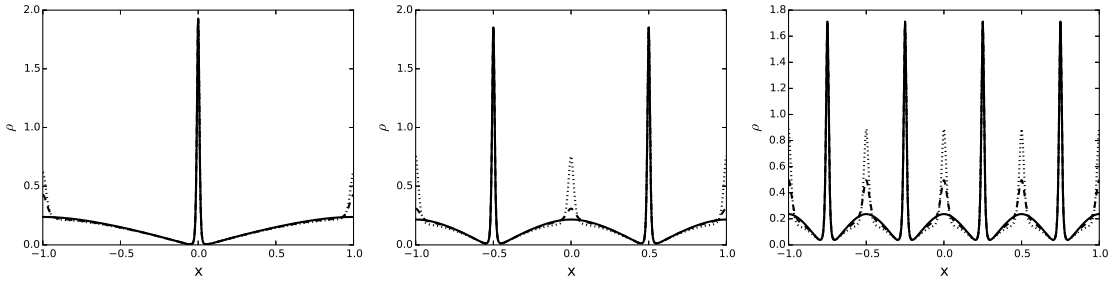

Figure 7. Time evolution of criminal density ρ for spatial patterns found by continuation beyond the fold point. Parameter values are $\epsilon = 0.01$, $\gamma = 2$, $\alpha = 1$, and $\ell = 1$. The values of D are $D = 2.0$, 0.5, 0.1 for the left, center and right, subfigures, respectively. The dotted, dashed and solid curves shows the solution at $t = 0$, 15, 100, respectively. We find that the plots at $t = 100$ all overlap exactly with those of the linearly stable patterns proved in §3 with parameter values given above.

or $K = 4$, interior hotspots. The goal of performing this codimension-two continuation to trace the curves $D_{\text{fold},K}(\epsilon)$ was to establish evidence for the conjecture that $\lim_{\epsilon\to 0} D_{\text{fold},K}(\epsilon) = D_{\text{crit},K}$, and to find a range of small ϵ where the agreement between $D_{\text{fold},K}$ and $D_{\text{crit},K}$ is close.

The results of this codimension-two computation are shown in Fig. 8. From this figure, we observe that the "almost" straight solid curves for the numerically computed values of $D_{\text{fold},K}(\epsilon)$ versus ϵ does seem to extrapolate as $\epsilon \to 0$ to the leading-order limiting critical value of §2. Due to numerical resolution difficulties, we were not able to perform computations for smaller values of ϵ than shown in Fig. 8. However, these computational results do give clear numerical evidence for the conjecture that $\lim_{\epsilon\to 0} D_{\text{fold},K}(\epsilon) = D_{crit,K}$ for $K = 1, 2, 4$. An analytical justification that $D_{crit,K}$ does in fact correspond to a fold point is given in the analysis of hotspot insertion phenomena in § 5.1 below. In Fig. 8, we also plot the improved approximation for $D_{crit,K}$ versus ϵ (dashed curves), as given in (5.28), that will be derived from the higher-order asymptotic theory of §5.

Finally, from the plots of A versus x in Fig. 8 at selected values of ϵ, we observe that when ϵ is only moderately small the steady-state solution more closely resembles a sinusoidal pattern than a pattern of localized hotspots.

5 The Steady-State Hotspot Solution: Higher-Order Theory

In this section we present a more refined asymptotic theory than that given in §2 to construct a steady-state hotspot solution centered at the origin on the interval $|x| \le \ell$. The results from this higher-order theory provide a rather close asymptotic prediction of the saddle-node bifurcation point observed in §4, as well as providing the error terms

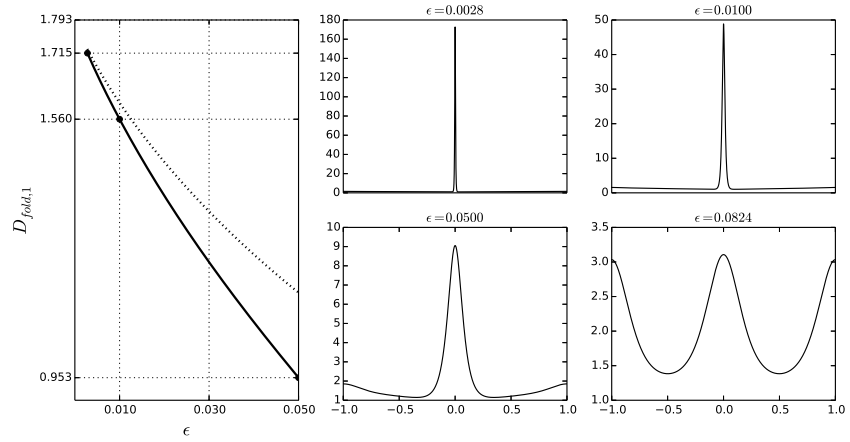

(a)

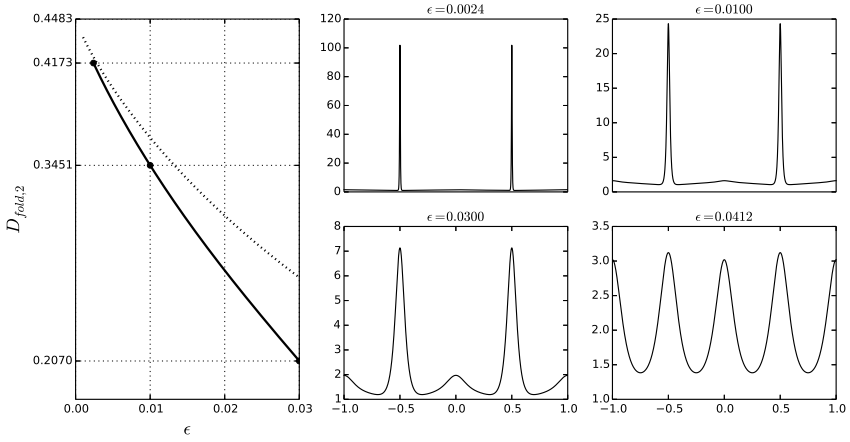

(b)

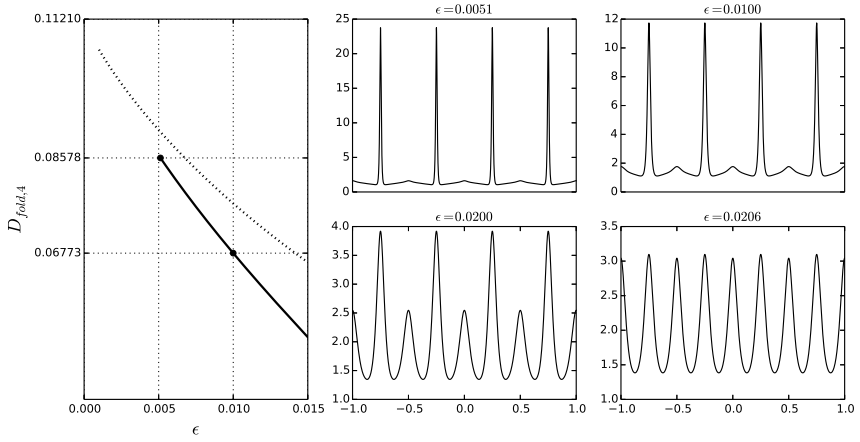

(c)

Figure 8. For the parameter set $\gamma = 2$, $\alpha = 1$, and $\ell = 1$, the solid curves on the left of each of (a), (b), and (c), for $K = 1$, $K = 2$, and $K = 4$, interior hotspots, respectively, show the fold point values $D_{\text{fold},K}(\epsilon)$ associated with the small norm solution branch of $A(\ell)$ versus D. The top tick-mark on the vertical axes in these plots are the approximate values $D_{\text{crit},1} \approx 1.793$, $D_{\text{crit},2} \approx 0.448$, and $D_{\text{crit},4} \approx 0.112$ from the leading-order theory of §2. The dashed curves in each of (a), (b), and (c), are the asymptotic results (5.28) for the fold point value for D, as predicted by the higher-order asymptotic theory of §5. For each of the three sets, the numerically computed A versus x is plotted on $|x| \leq 1$ at four values of ϵ. At the larger values of ϵ the pattern is essentially sinusoidal.

associated with the leading-order theory. In addition, this more refined asymptotic analysis is essential for the analysis in §6, where an ODE-DAE system for the slow time evolution of a collection of hotspots is derived.

In the inner region, where $y = \epsilon^{-1}x$ and $y = \mathcal{O}(1)$, we pose a two-term expansion for A as

$$A \sim A_0/\epsilon + A_1 + \dots\,, \qquad V \sim \epsilon^2 V_\epsilon\,.$$

Upon substituting this expansion into (1.5), and retaining the dominant correction terms we obtain

$$\left(A_{0yy} - A_0 + V_\epsilon A_0^3\right) + \epsilon\left(A_{1yy} - A_1 + 3V_\epsilon A_0^2 A_1 + \alpha\right) + \cdots = 0\,, \tag{5.1 a}$$

$$D\left[\left(A_0^2 + 2\epsilon A_0 A_1\right)V_{\epsilon y}\right]_y - \epsilon V_\epsilon\left(A_0^3 + 3A_0^2 A_1\epsilon\right) + \epsilon^2(\gamma - \alpha) + \cdots = 0\,. \tag{5.1 b}$$

This suggests that we expand $V_\epsilon = V_0 + \epsilon V_1 + \cdots$. Upon substituting this expansion into (5.1), and collecting powers of ϵ, we obtain our leading-order result that V_0 is an unknown constant and $A_0 = w/\sqrt{V_0}$, where $w(y) = \sqrt{2}\,\mathrm{sech}\, y$ is the homoclinic solution of (2.3). At next order, we obtain that $A_1(y)$ and $V_1(y)$ on $-\infty < y < \infty$ satisfy

$$A_{1yy} - A_1 + 3A_0^2 A_1 V_0 = -\alpha - V_1 A_0^3\,, \qquad D\left[A_0^2 V_{1y}\right]_y = V_0 A_0^3\,. \tag{5.2}$$

Then, upon substituting $A_0 = w/\sqrt{V_0}$ into (5.2), we conclude that

$$L_0 A_1 \equiv A_{1yy} - A_1 + 3w^2 A_1 = -\alpha - \frac{V_1}{V_0^{3/2}}w^3\,, \qquad \left[w^2 V_{1y}\right]_y = \frac{\sqrt{V_0}}{D}w^3\,. \tag{5.3}$$

A key step in analyzing the inner region is to determine the far-field asymptotic behavior as $y \to +\infty$ for the solution to (5.3). Since $w(y) \sim 2\sqrt{2}e^{-y}$ as $y \to \infty$, it readily follows upon integrating the V_1-equation that $V_1 = \mathcal{O}(e^{2y})$ as $y \to \infty$. Then, since $w^3 V_1 \to 0$ as $y \to \infty$, it follows from the A_1-equation in (5.3) that $A_1 \to \alpha$ as $y \to \infty$. These simple results show that the V_ϵ-expansion $V_\epsilon = V_0 + \epsilon V_1 + \cdots$ becomes disordered when $y = \mathcal{O}(-(1/2)\log\epsilon)$, while the far-field as $y \to \infty$ of the A-expansion $A = w/\left[\epsilon\sqrt{V_0}\right] + A_1 \sim \epsilon^{-1}2\sqrt{2}e^{-y} + \alpha$ becomes disordered when $y = \mathcal{O}(-\log\epsilon)$.

As a result, for $y > 0$, we will need to introduce two additional inner layers before we are finally able to match to the outer solution. For $\epsilon \to 0$, we define the *mid-inner layer* by $y = -(1/2)\log\epsilon + \mathcal{O}(1)$ and the *knee layer* by $y = -\log\epsilon + \mathcal{O}(1)$. The asymptotic solution in the knee layer can then be matched to the outer solution valid on $0 < x < \ell$. By symmetry, a similar construction can be done for $y < 0$. In Fig. 9 we plot the full numerical steady-state solution for V, as computed from (1.5), showing the knee behavior of V for $\gamma = 2$, $\alpha = 1$, $D = 2$, $\epsilon = 0.01$, and $\ell = 1$.

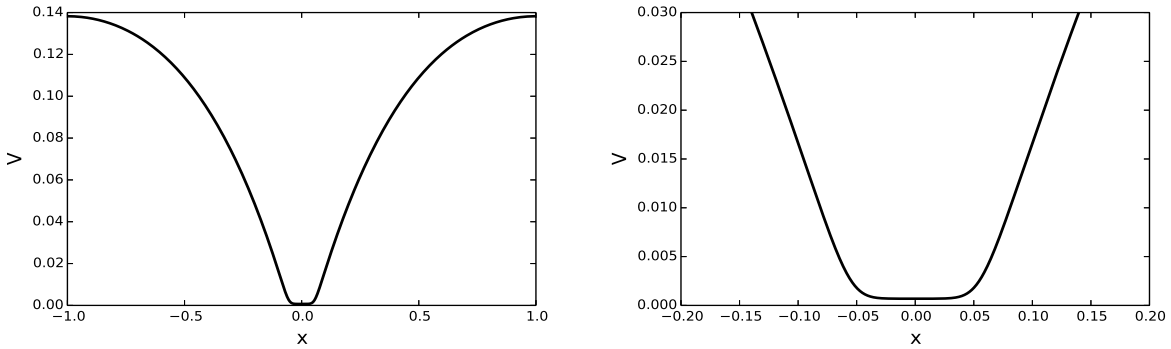

Figure 9. Plot of the full numerical solution to the steady-state problem (1.5) showing the knee behavior of V for $\gamma = 2$, $\alpha = 1$, $D = 2$, $\epsilon = 0.01$, and $\ell = 1$. The figure on the right is a zoom of the one on the left.

The asymptotic matching of the expansions of the solution across the mid-inner and knee layers will specify the appropriate far field behavior for the solution V_1 to (5.3) in the form

$$V_1 \sim b_+ e^{2|y|}\,, \quad \text{as} \quad |y| \to \infty\,, \tag{5.4}$$

for a certain constant b_+ that is, ultimately, determined by the outer solution. In this way, we can decompose the inner correction term V_1, satisfying (5.3), as $V_1(y) = V_{10} + V_{1p}(y)$, where V_{10} is a constant to be determined and where $V_{1p}(y)$ satisfies

$$\left[w^2 V_{1py}\right]_y = \frac{\sqrt{V_0}}{D}w^3\,, \qquad -\infty < y < \infty\,; \qquad V_{1p} \sim b_+ e^{2|y|} \quad \text{as} \quad |y| \to \infty\,; \quad V_{1p}(0) = 0\,. \tag{5.5}$$

Upon integrating (5.5) on $-\infty < y < \infty$, we conclude that a solution to (5.5) exists if and only if

$$\frac{\sqrt{V_0}}{D}\int_{-\infty}^{\infty} w^3\,dy = \lim_{y\to+\infty}\left(w^2V_{1py}\right) - \lim_{y\to-\infty}\left(w^2V_{1py}\right)\,. \tag{5.6}$$

By using the limiting behaviors of w and V_{1p} as $|y|\to\infty$, together with $\int_{-\infty}^{\infty} w^3\,dy = \sqrt{2}\pi$, we obtain that

$$\frac{\sqrt{V_0}}{D} = \frac{16\sqrt{2}}{\pi}b_+\,. \tag{5.7}$$

With V_0 determined in this way, the solution to (5.5) is even in y and given explicitly by

$$V_{1p} = \frac{\sqrt{V_0}}{D}\left(\frac{1}{\sqrt{2}}\left(\cosh y - 1\right) + \sqrt{2}\int_0^y \cosh^2(s)\tanh^{-1}\left[\tanh\left(\frac{s}{2}\right)\right]\,ds\right)\,. \tag{5.8}$$

To determine b_+, we now proceed by analyzing the two additional inner layers. We begin with the knee-layer, defined by $y = -\log\epsilon + \mathcal{O}(1)$, which can be matched to the limiting behavior as $x\to 0^+$ of the outer solution. In the knee-layer, we introduce the new variables $\hat{A}$, $\hat{V}$, and z by

$$A = \hat{A}(z)\,, \qquad V = \epsilon\hat{V}(z)\,, \qquad y = -\log\epsilon + z\,,$$

with $z = \mathcal{O}(1)$, so that $x = -\epsilon\log\epsilon + \epsilon z$. In terms of these new variables, (1.5) becomes

$$\hat{A}_{zz} - \hat{A} + \epsilon\hat{V}\hat{A}^3 + \alpha = 0\,, \qquad D\left(\hat{A}^2\hat{V}_z\right)_z - \epsilon^2\hat{V}\hat{A}^3 + \epsilon(\gamma-\alpha) = 0\,. \tag{5.9}$$

We substitute the expansion $\hat{A} = \hat{A}_0 + \cdots$ and $\hat{V} = \hat{V}_0 + \cdots$ into (5.9) to obtain that $\hat{A}_{0zz} - \hat{A}_0 = -\alpha$. The solution for $\hat{A}_0$ that agrees with the far-field behavior of the inner solution for A is

$$\hat{A}_0 = ce^{-z} + \alpha\,, \qquad c \equiv \frac{2\sqrt{2}}{\sqrt{V_0}}\,. \tag{5.10}$$

In contrast, $\hat{V}_0(z)$ satisfies

$$\left[\hat{A}_0^2\hat{V}_{0z}\right]_z = 0\,, \qquad -\infty < z < \infty\,. \tag{5.11}$$

To determine the appropriate far-field behavior as $z\to+\infty$ for (5.11), we expand the leading-order outer solution $v_0(x)$ of §2 as $x\to 0$, and then rewrite the expression in terms of z to obtain the matching condition

$$\epsilon\hat{V} \sim \epsilon v_{0x}(0^+)z + (-\epsilon\log\epsilon)v_{0x}(0^+) + \cdots\,. \tag{5.12}$$

The dominant constant term of order $\mathcal{O}(-\epsilon\log\epsilon)$ in (5.12) cannot be accounted for by the knee solution. Instead, we must introduce a switchback term of order $\mathcal{O}(-\epsilon\log\epsilon)$ into the outer expansion. More specifically, the outer expansion on $0 < x < \ell$ must have the form

$$A \sim a_0 + (-\epsilon\log\epsilon)\,a_1 + \epsilon a_2 + \cdots\,, \qquad V \sim v_0 + (-\epsilon\log\epsilon)\,v_1 + \epsilon v_2 + \cdots\,, \tag{5.13}$$

with $v_1(0^+) = -v_{0x}(0^+)$, chosen to eliminate the constant term in (5.12)

Therefore, to match the knee solution $\hat{V}_0$ to the near-field behavior (5.12) of the outer solution we require that $\hat{V}_{0z}\sim v_{0x}(0^+)$ as $z\to\infty$. In contrast, to match the knee solution $\hat{V}_0$ to the mid-inner solution where $V = \mathcal{O}(\epsilon^2)$, we need that $\hat{V}_0\to 0$ as $z\to-\infty$. Thus, we must solve (5.11) subject to

$$\hat{V}_{0z}\sim v_{0x}(0^+)\,, \quad \text{as} \quad z\to+\infty\,; \qquad \hat{V}_0\to 0\,, \quad \text{as} \quad z\to-\infty\,. \tag{5.14}$$

Given the decay as $z\to-\infty$ and linear ramp as $z\to+\infty$, it is now clear why we refer to $\hat{V}_0$ as the *knee solution*. Upon using (5.10) for $\hat{A}_0$, a first integral of (5.11), which satisfies $\hat{V}_{0z}\sim v_{0x}(0^+)$ as $z\to+\infty$, is

$$\hat{V}_{0z} = \frac{\alpha^2 v_{0x}(0^+)}{\left(ce^{-z}+\alpha\right)^2}\,. \tag{5.15}$$

Upon integrating (5.15) and imposing the condition that $\hat{V}_0\to 0$ as $z\to-\infty$, we can determine the knee solution

explicitly as

$$\hat{V}_0 = v_{0x}(0^+)\left(\log(c+\alpha e^z) + \frac{c}{(c+\alpha e^z)} - 1 - \log c\right). \tag{5.16}$$

From the explicit solution in (5.16), we obtain as $z \to +\infty$ that

$$\hat{V}_0 \sim v_{0x}(0^+)z + \left[\log\left(\frac{\alpha}{c}\right) - 1\right] v_{0x}(0^+). \tag{5.17}$$

This second term in (5.17) provides a matching condition for the outer correction v_2 in (5.13) of the form

$$v_2(0^+) = \left[\log\left(\frac{\alpha}{c}\right) - 1\right] v_{0x}(0^+). \tag{5.18}$$

Alternatively, as $z \to -\infty$, we readily calculate from (5.16) that

$$\hat{V}_0 \sim \frac{\alpha^2 v_{0x}(0^+)}{2c^2} e^{2z}, \quad \text{as} \quad z \to -\infty. \tag{5.19}$$

Equation (5.19) yields the far-field behavior of the mid-inner solution for V, which we now construct.

To analyze the mid-inner layer, which is between the inner and knee-layer regions, we introduce the new variables $\tilde{A}$, $\tilde{V}$, and η by

$$A = \tilde{A}(\eta), \qquad V = \epsilon^2 \tilde{V}(\eta), \qquad y = -\frac{1}{2}\log\epsilon + \eta,$$

with $\eta = \mathcal{O}(1)$, so that $x = -(\epsilon/2)\log\epsilon + \epsilon\eta$. In this layer, where $V = \mathcal{O}(\epsilon^2)$, the asymptotic order of V is the same as that in the inner layer. Therefore, it is the knee layer that has allowed for the fast transition in V from an $\mathcal{O}(\epsilon^2)$ scale to an $\mathcal{O}(\epsilon)$ scale, which is then matchable to the outer solution. Upon substituting these new variables into (1.5), we obtain to leading-order that $\tilde{A} \sim \tilde{A}_0 + \cdots$ where

$$\tilde{A}_0 = \frac{c}{\sqrt{\epsilon}} e^{-\eta} + \alpha, \qquad c \equiv \frac{2\sqrt{2}}{\sqrt{V_0}},$$

and that $\tilde{V} = \tilde{V}_0 + \cdots$, where $\tilde{V}_0$ satisfies

$$\left[e^{-2\eta}\tilde{V}_{0\eta}\right]_\eta = 0, \qquad -\infty < \eta < \infty. \tag{5.20}$$

The solution to (5.20) that matches as $\eta \to +\infty$ to the asymptotics (5.19) of the knee solution, and that satisfies $\tilde{V}_0 \sim V_0$ as $\eta \to -\infty$ in order to match to inner layer solution, is simply

$$\tilde{V}_0 = \frac{\alpha^2 v_{0x}(0^+)}{2c^2} e^{2\eta} + V_0. \tag{5.21}$$

Finally, we write (5.21) in terms of the inner variable y as $\eta = y + (1/2)\log\epsilon$ to obtain the following matching condition as $y \to +\infty$ for the inner solution:

$$V \sim \epsilon^2 \tilde{V}_0 \sim \epsilon^2 V_0 + \epsilon^3 \left(\frac{\alpha^2 v_{0x}(0^+)}{2c^2}\right) e^{2y}.$$

In this way, we conclude that the solution $V_{1p}(y)$ to (5.5) must satisfy

$$V_{1p} \sim b_+ e^{2y}, \quad \text{as} \quad y \to +\infty, \qquad b_+ \equiv \frac{\alpha^2 v_{0x}(0^+)}{2c^2}, \qquad c \equiv \frac{2\sqrt{2}}{\sqrt{V_0}}. \tag{5.22}$$

This rather intricate asymptotic construction has served to identify the constant b_+ in (5.5), which can then be used in (5.7) to determine the leading-order constant V_0. In fact, upon substituting (5.22) into (5.7), and solving for V_0, we obtain

$$\sqrt{V_0} = \frac{\pi}{\sqrt{2}\alpha^2 D v_{0x}(0^+)}. \tag{5.23}$$

Then, by using (2.18) for $v_{0x}(0^+)$ in (5.23), we recover the leading order result (2.21) for V_0, as derived previously in §2. A higher order approximation for $V(0)$, based on analyzing correction terms to V_0, is derived in (5.27) below.

We remark that although the leading-order theory of §2 was also able to determine V_0 by simply integrating the

V-equation in (1.5) over an intermediate, but otherwise unspecified, length-scale δ with $\epsilon \ll \delta \ll 1$, as was done in (2.19), the more refined asymptotic approach in this section provides the gradient information in V that is essential in §6 for deriving a DAE system for the slow dynamics of a hotspot. Moreover, this asymptotic construction has shown how the knee-layer solution allows V to make a fast transition between $\mathcal{O}(\epsilon^2)$ and $\mathcal{O}(\epsilon)$ scales.

Next, we proceed to analyze the correction terms in the outer region of the form (5.13). Upon substituting the A-expansion of (5.13) into (1.5), we obtain that $V = g(A)$ to both $\mathcal{O}(-\epsilon\log\epsilon)$ and $\mathcal{O}(\epsilon)$ terms, where $g(A)$ is defined in (2.4). Therefore, $v_j = g'(a_0)a_j$ for $j = 1, 2$, and hence the problems for a_1 and a_2 can be obtained by replacing a_0 in (2.5) with $a_0 + (-\epsilon\log\epsilon)a_1 + \epsilon a_2$, and then performing a simple Taylor series expansion. To determine the boundary conditions for a_1 and a_2, we use $a_0(0^+) = \alpha$, $g'(\alpha) = \alpha^{-3}$, and $v_j = g'(a_0)a_j$ for $j = 1, 2$, together with the matching conditions $v_1(0^+) = -v_{0x}(0^+)$ and $v_2(0^+) = \left[\log\left(\frac{\alpha}{c}\right) - 1\right] v_{0x}(0^+)$, to identify conditions for a_1 and a_2 at $x = 0^+$. In this way, we obtain that $a_0(x)$ satisfies (2.5), while $a_1(x)$ and $a_2(x)$ satisfy

$$D\left[f(a_0)a_1\right]_{xx} = a_1\,, \qquad 0 < x < \ell\,; \qquad a_1(0^+) = -a_{0x}(0^+)\,, \quad a_{1x}(\ell) = 0\,, \tag{5.24 a}$$

$$D\left[f(a_0)a_2\right]_{xx} = a_2\,, \qquad 0 < x < \ell\,; \qquad a_2(0^+) = \left[\log\left(\frac{\alpha}{c}\right) - 1\right] a_{0x}(0^+)\,, \quad a_{2x}(\ell) = 0\,. \tag{5.24 b}$$

Our key observation is that instead of solving (2.5) and (5.24) recursively for a_0, a_1, and a_2, these outer approximations are contained in the solution to a *renormalized outer problem* for $a_\epsilon(x)$, formulated as

$$D\left[f(a_\epsilon)a_{\epsilon x}\right]_x = a_\epsilon - \gamma\,, \qquad x_\epsilon < x < \ell\,; \qquad a_\epsilon(x_\epsilon) = \alpha\,, \quad a_{\epsilon x}(\ell) = 0\,, \tag{5.25 a}$$

where $x_\epsilon > 0$ is defined by

$$x_\epsilon = (-\epsilon\log\epsilon)\,x_1 + \epsilon x_2\,; \qquad x_1 = 1\,, \quad x_2 \equiv 1 - \log\left(\frac{\alpha}{c}\right)\,, \quad c \equiv \frac{2\sqrt{2}}{\sqrt{V_0}}\,. \tag{5.25 b}$$

By formally expanding the solution $a_\epsilon(x)$ to (5.25) in the gauge functions of (5.13), we readily recover the problems (2.5) and (5.24) for a_0, a_1, and a_2. Therefore, the effect on the outer solution of the knee layer is that one needs to account for an inner region that is $\mathcal{O}(-\epsilon\log\epsilon)$ thick. The expression (5.25 b) also shows that the outer solution has a weak dependence on the amplitude of the hotpsot, mediated by V_0. One key advantage of using the renormalized problem (5.25) is that the leading-order theory of §2 can still be used provided that we simply replace ℓ with $\ell - x_\epsilon$. This idea of renormalizing the outer solution to account for the switchback term is vaguely similar to the renormalization method proposed in [**7**] for analyzing weakly nonlinear oscillators.

Next, we use the renormalized problem (5.25) to determine an improved approximation $V_{0\epsilon}$ for $\epsilon^{-2}V(0)$. This new approximation consists of two weakly coupled nonlinear algebraic equations for $\mu_\epsilon \equiv a_\epsilon(\ell)$ and $V_{0\epsilon}$. To determine the first relation between μ_ϵ and $V_{0\epsilon}$ we integrate the V-equation in (1.5) from $-x_\epsilon < x < x_\epsilon$ to obtain, in place of (2.19), that

$$2D\alpha^2 v_{\epsilon x}(x_\epsilon) = 2\sqrt{2D}\sqrt{G(\mu_\epsilon) - G(\alpha)} \sim \frac{1}{\sqrt{V_{0\epsilon}}}\int_{-\infty}^{\infty} w^3\,dy - 2x_\epsilon(\gamma - \alpha)\,. \tag{5.26}$$

Here we have used $v_{\epsilon x}(x_\epsilon) = g'(\alpha)a_{\epsilon x}(x_\epsilon)$, where $g'(\alpha) = \alpha^{-3}$ and $a_{\epsilon x}(x_\epsilon)$ is obtained from a first integral of the renormalized problem (5.25). By solving the expression above for $V_{0\epsilon}$, we obtain our first relation

$$V_{0\epsilon} = \frac{\pi^2}{2\left[\sqrt{2D}\left(\sqrt{G(\mu_\epsilon) - G(\alpha)}\right) + (\gamma - \alpha)x_\epsilon\right]^2}\,. \tag{5.27 a}$$

The second relation is obtained by replacing μ and ℓ in (2.12) with μ_ϵ and $\ell - x_\epsilon$, where x_ϵ is defined in (5.25 b). This yields

$$\chi(\mu_\epsilon) = \sqrt{\frac{2}{D}}\,(\ell - x_\epsilon)\,, \qquad x_\epsilon = (-\epsilon\log\epsilon) + \epsilon\left(1 + \log\left(\frac{2\sqrt{2}}{\alpha}\right) - \log\sqrt{V_{0\epsilon}}\right)\,, \tag{5.27 b}$$

where $\chi(\mu)$ is defined in (2.11).

The system (5.27) is a weakly coupled nonlinear algebraic system for $V_{0\epsilon}$ and $\mu_\epsilon \equiv a_\epsilon(\ell)$, where the coupling arises through the fact that x_ϵ depends weakly on $V_{0\epsilon}$. By solving this weakly coupled system using Newton's method for $\gamma = 2$, $\alpha = 1$, $D = 2$, and $\ell = 1$, in the right panel of Fig. 4 (thin dotted curve) we showed that $V_{0\epsilon}$ compares more

favorably with the full numerical result than does the leading-order result V_0. Similarly, as was shown in the left panel of Fig. 4, the renormalized approximation $\sqrt{2}/\sqrt{V_{0\epsilon}}$ for $\epsilon A(0)$ compares rather well with full numerics when ϵ is small.

Finally, to determine an improved approximation, labelled by $D_{\text{crit},\epsilon}$, for the minimum value of D for which a steady-state hotspot solution on $|x| \le \ell$ exists, we simply set $\mu_\epsilon = 3\alpha/2$ in (5.27) and solve the resulting system for $D = D_{\text{crit},\epsilon}$ and $V_{0\epsilon}$. In particular, for a single hotspot solution on $|x| \le \ell$ we have

$$D_{\text{crit},\epsilon} \equiv \frac{2(\ell - x_\epsilon)^2}{\chi^2_{\max}}\,, \tag{5.28 a}$$

where $\chi_{\max} \equiv \chi\,(3\alpha/2)$, and $\chi(\mu)$ is defined in (2.11). In addition, the minimum value of D for a pattern of K interior hotspots on the domain $|x| \le 1$, is obtained by setting $\ell = 1/K$ into (5.28 *a*). This yields the critical thresholds

$$D_{\text{crit},\epsilon,K} = \frac{2(K^{-1} - x_\epsilon)^2}{\chi^2_{\max}}\,. \tag{5.28 b}$$

In Fig. 8 of §4 we showed that the improved approximation $D_{\text{crit},\epsilon,K}$ for the minimum value of D for a steady-state pattern of K-interior hotspots on the domain $|x| \le 1$ compares rather well with the full numerical results as ϵ is decreased. In comparison with the ϵ-independent results of (2.17) of §2 for the minimum value of D as obtained from the leading-order theory, our improved theory on $|x| \le 1$ when $\gamma = 2$, $\alpha = 1$, and $\epsilon = 0.01$, yields

$$D_{\text{crit},\epsilon,1} \approx 1.5985\,, \qquad D_{\text{crit},\epsilon,2} \approx 0.3646\,, \qquad D_{\text{crit},\epsilon,4} \approx 0.0771\,. \tag{5.29}$$

As seen from Fig. 8 and (4.1), these improved approximations for the minimum value of D compare rather favorably with full numerical results. Moreover, in comparing (5.29) with the results (2.17) from the leading-order theory of §2, it is evident that the effect of the ϵ-dependent correction terms is rather significant even at $\epsilon = 0.01$.

For a one-hotspot solution, in §5.1 below we construct a new boundary layer near $x = \ell$ when $D \approx D_{\text{crit},\epsilon}$. For this analysis, we need to determine the local behavior near $x = \ell$ of the solution to (5.25) when $D = D_{\text{crit},\epsilon}$, corresponding to when $a_\epsilon(\ell) = a_{0c} \equiv 3\alpha/2$. Near $x = l$, we put $a_\epsilon = a_{0c} + \bar{a}(x)$, where $\bar{a} \ll 1$ and $\bar{a}(\ell) = 0$. Upon substituting into (5.25), we obtain near $x = \ell$ that $[f'(a_{0c})\bar{a}\bar{a}_x]_x \sim (a_{0c} - \gamma)/D_{\text{crit},\epsilon}$, where $f'(a_{0c}) = -2/a^2_{0c}$. Therefore, near $x = \ell$, we have

$$(\bar{a}\bar{a}_x)_x \sim \frac{a^2_{0c}(\gamma - a_{0c})}{2D_{\text{crit},\epsilon}}\,.$$

Upon integrating this equation and imposing $\bar{a}(\ell) = 0$, we get for x near ℓ that

$$\left(\frac{1}{2}\bar{a}^2\right)_x \sim \beta a^2_{0c}(x - \ell)\,, \qquad \beta \equiv \frac{(\gamma - a_{0c})}{2D_{\text{crit},\epsilon}}\,.$$

Integrating once more, and imposing $\bar{a}(\ell) = 0$, we obtain that $\bar{a} \sim \sqrt{\beta} a_{0c}(x - \ell)$ as $x \to \ell^-$. We conclude that as $x \to \ell^-$, the local behavior of the solution to (5.25) when $D = D_{\text{crit},\epsilon}$ is

$$a_\epsilon(x) \sim a_{0c} + \beta^{1/2} a_{0c}(x - \ell)\,, \quad \text{as} \quad x \to \ell^-\,, \qquad \text{where} \qquad a_{0c} \equiv \frac{3\alpha}{2}\,, \qquad \beta \equiv \frac{(\gamma - a_{0c})}{2D_{\text{crit},\epsilon}}\,. \tag{5.30}$$

Since, when $a_\epsilon(\ell) = 3\alpha/2$, the solution $a_\epsilon(x)$ no longer satisfies the no-flux condition $a_{\epsilon,x}(\ell) = 0$, we need to construct a new boundary layer near $x = \ell$. This is done in the next sub-section.

5.1 Hotspot Insertion Analysis: A Normal Form Equation

The full numerical computations of §4, and the local analysis in (5.30) of §5, motivate the need for constructing a new boundary layer solution near the endpoints $x = \pm\ell$ when D is near the critical value $D_{\text{crit},\epsilon}$. This boundary layer analysis, which is shown below to generate multiple solutions in the boundary layer region, characterizes the onset of the peak insertion phenomena at the edges of the domain. We show that the overall mechanism for the creation of new hotspots is markedly similar to the analysis of [**20**] for the onset of self-replication behavior of mesa patterns. Indeed, we derive a normal form equation, characterizing the local behavior of the peak insertion process, that has the same structure as that derived in [**20**]. However, as an extension of the analysis of [**20**], we derive a formula, valid near the critical threshold $D_{\text{crit},\epsilon}$, that shows analytically how the solution multiplicity associated with the boundary layer solution near $x = \ell$ leads to a fold-point behavior in the bifurcation diagram of $A(\ell)$ versus D.

To analyze the onset of the peak insertion process, we first write the outer problem for the steady-state problem (1.5) in the form

$$\epsilon^2 A_{xx} + A^3\left[V - g(A)\right] = 0\,, \qquad D\left[A^2 V_x\right]_x - A + \gamma - A^3\left[V - g(A)\right] = 0\,, \tag{5.31}$$

on $x_\epsilon < x < \ell$, where $g(A)$ is defined in (2.4). We let $a_\epsilon(x)$ and $D_{\rm crit,\epsilon}$ denote the solution to the renormalized outer problem (5.25) at the critical value where $a_\epsilon(\ell) = 3\alpha/2$. In terms of $a_\epsilon(x)$, $v_\epsilon(x)$ is given by $v_\epsilon(x) = g(a_\epsilon(x))$, where $g(A)$ is defined in (2.4). In the outer region, away from both the hotspot core and a thin boundary layer to be constructed near $x = \ell$, we expand the outer solution to (5.31), together with $\Lambda \equiv 1/D$, as

$$A = a_\epsilon + \nu a_{\epsilon,1} + \cdots\,, \qquad V = v_\epsilon + \nu v_{\epsilon,1} + \cdots\,, \qquad \Lambda \equiv \frac{1}{D} = \Lambda_\epsilon + \nu\Lambda_{\epsilon,1} + \cdots\,, \tag{5.32}$$

where the gauge function $\nu \ll 1$ and the constant $\Lambda_{\epsilon,1}$ are to be determined. By expanding $D = D_{\rm crit,\epsilon} + \nu D_{\epsilon,1} + \cdots$, and then comparing with the expansion of Λ in (5.32), we identify that

$$D_{\rm crit,\epsilon} = \frac{1}{\Lambda_\epsilon}\,, \qquad D_{\epsilon,1} = -\frac{\Lambda_{\epsilon,1}}{\Lambda_\epsilon^2}\,. \tag{5.33}$$

We substitute (5.32) into (5.31) and collect powers of ν. Assuming that $\nu \gg \mathcal{O}(\epsilon^2)$, we obtain that a_ϵ satisfies the renormalized problem (5.25) with $a_\epsilon(\ell) = 3\alpha/2$, and that $a_{\epsilon,1}$ satisfies

$$\left[f(a_\epsilon)a_{\epsilon,1}\right]_{xx} - \Lambda_\epsilon a_{\epsilon,1} = \Lambda_{\epsilon,1} a_\epsilon\,, \qquad x_\epsilon < x < \ell\,; \qquad a_{\epsilon,1}(x_\epsilon) = 0\,. \tag{5.34}$$

The asymptotic boundary condition for $a_{\epsilon,1}$ as $x \to \ell^-$ will be derived below upon matching to the boundary layer solution to be constructed near $x = \ell$.

To construct the thin boundary layer near $x = \ell$, we begin by introducing the new variables $\mathcal{A}_1$, $\mathcal{V}_1$, and z, by

$$A = a_{0c} + \delta\mathcal{A}_1(z) + \cdots\,, \qquad V = v_{0c} + \delta^2\mathcal{V}_1(z) + \cdots\,, \qquad z \equiv \sigma^{-1}[\ell - x]\,, \tag{5.35}$$

where $a_{0c} \equiv 3\alpha/2$ and $v_{0c} \equiv g(a_{0c}) = 4/(27\alpha^2)$. Here the gauge functions $\sigma \ll 1$ and $\delta \ll 1$ are to be determined. The choice of different scales for A and V is motivated by the fact that $g'(a_{0c}) = 0$. We substitute (5.35) into (5.31), and after a Taylor expansion of $g(A)$, we obtain that

$$\frac{\epsilon^2\delta}{\sigma^2}\mathcal{A}_{1zz} + \delta^2 a_{0c}^3\left[\mathcal{V}_1 - \frac{1}{2}g''(a_{0c})\mathcal{A}_1^2\right] + \cdots = 0\,, \qquad \frac{a_{0c}^2}{\sigma^2}\delta^2\mathcal{V}_{1zz} = \Lambda_\epsilon\left(a_{0c} - \gamma\right) + \cdots\,, \tag{5.36}$$

where from (2.4) we calculate that

$$g''(a_{0c}) = -2a_{0c}^{-4}\,, \qquad a_{0c} \equiv \frac{3\alpha}{2}\,. \tag{5.37}$$

To balance the terms in (5.36) we must relate σ and δ to ϵ by $\delta = \sigma$ and $\delta\sigma^2 = \epsilon^2$, which yields that

$$\delta = \epsilon^{2/3}\,, \qquad \sigma = \epsilon^{2/3}\,. \tag{5.38}$$

With this choice, (5.36) reduces to leading order on $0 < z < \infty$ to

$$\mathcal{A}_{1zz} + a_{0c}^3\left(\mathcal{V}_1 + \frac{\mathcal{A}_1^2}{a_{0c}^4}\right) = 0\,, \qquad \mathcal{V}_{1zz} = -\frac{2\beta}{a_{0c}^2}\,, \qquad \beta \equiv \frac{\Delta_\epsilon}{2}\left(\gamma - a_{0c}\right) > 0\,. \tag{5.39}$$

In order to satisfy the no-flux boundary conditions for A and V on $x = \ell$ we must impose that $\mathcal{A}_{1z}(0) = \mathcal{V}_{1z}(0) = 0$.

Upon integrating the $\mathcal{V}_1$-equation, and imposing $\mathcal{V}_{1z}(0) = 0$, we get that $\mathcal{V}_1 = \mathcal{V}_{10} - \beta z^2/a_{0c}^2$. Then, from the $\mathcal{A}_1$-equation in (5.39), we obtain

$$\mathcal{A}_{1zz} + a_{0c}^3\left(-\frac{\beta}{a_{0c}^2}z^2 + \mathcal{V}_{10} + \frac{\mathcal{A}_1^2}{a_{0c}^4}\right) = 0\,, \qquad 0 < z < \infty\,, \tag{5.40}$$

where $\mathcal{V}_{10}$ is an arbitrary constant. To obtain our normal form equation we eliminate as many parameters as possible in (5.40) by rescaling z and $\mathcal{A}_1$ by

$$\mathcal{A}_1 = bU\,, \qquad z = \xi y\,. \tag{5.41 a}$$

By choosing

$$\xi = \beta^{-1/6}\,, \qquad b = a_{0c}\beta^{1/3}\,, \tag{5.41 b}$$

we obtain that (5.40) transforms to the normal form equation

$$U_{yy} + U^2 - y^2 + \kappa = 0\,, \qquad 0 < y < \infty\,; \qquad U_y(0) = 0\,, \tag{5.42 a}$$

where the parameter κ is defined

$$\kappa \equiv a_{0c}^2 \beta^{-2/3} \mathcal{V}_{10}\,. \tag{5.42 b}$$

In order to match solutions to (5.42) with those in the outer region, we need that $U_y \to -1$ as $y \to +\infty$, which is consistent with the condition that $A_x > 0$ as $x \to \ell^-$.

Finally, in terms of the original variables, we obtain from (5.35), (5.38), and (5.41), that the boundary layer solution near $x = \ell$ is characterized by

$$A \sim a_{0c} + \epsilon^{2/3} a_{0c} \beta^{1/3} U(y)\,, \qquad V \sim v_{0c} + \epsilon^{4/3} \frac{\beta^{2/3}}{a_{0c}^2} \left(\kappa - y^2\right)\,, \qquad y \equiv \beta^{1/6} \epsilon^{-2/3} (\ell - x)\,, \tag{5.43}$$

where $a_{0c} \equiv 3\alpha/2$, $v_{0c} \equiv g(a_{0c}) = 4/(27\alpha^2)$, and β is defined in (5.39).

We observe that $-U$ satisfies exactly the equation (2.26) in [**20**]. The properties of solutions to (5.42) were established in Theorem 2 of [**20**], and we simply re-state this result here for the convenience of the reader.

Theorem 1 (From [**20**]) *In the limit $\kappa \to -\infty$, (5.42) admits exactly two solutions $U = U^{\pm}(y)$ with $U' < 0$ for $y > 0$, with the following uniform expansions:*

$$U^+ \sim -\sqrt{y^2 - \kappa}\,, \qquad U^+(0) \sim -\sqrt{-\kappa}\,, \tag{5.44 a}$$

$$U^- \sim -\sqrt{y^2 - \kappa}\left(1 - 3\,\mathrm{sech}^{\,2}\left(\frac{\sqrt{-\kappa}\, y}{\sqrt{2}}\right)\right)\,, \qquad U^-(0) \sim +\sqrt{-\kappa}\,. \tag{5.44 b}$$

These two solutions are connected. For any such solution, define s by $s \equiv U(0)$ and consider the solution branch $\kappa = \kappa(s)$. Then, $\kappa(s)$ has a unique (maximum) critical point at $s = s_{max}$ and $\kappa = \kappa_{max}$. Numerical computations yield that $\kappa_{max} \approx 1.46638$ and $s_{max} \approx 0.61512$.

A bifurcation diagram of κ versus $s \equiv U(0)$ for solutions to the normal form equation (5.42) is shown in the left panel of Fig. 10. In the right panel of Fig. 10 we plot the numerically computed solution $U(y)$ (solid curve), and the derivative $U'(y)$ (dashed curve), at a few selected values of $s = U(0)$.

We now proceed to analyze how the solution multiplicity in this boundary layer solution leads to a fold-point behavior in the bifurcation diagram of $A(\ell)$ versus D. This analysis is new and was not done in [**20**]. To do so, we first need to determine the far-field behavior as $y \to \infty$ for any solution of (5.42). We let $U = -\sqrt{y^2 - \kappa} + \bar{U}$ in (5.42), where $\bar{U} \ll 1$, to obtain that

$$\bar{U}_{yy} - \left(2\sqrt{y^2 - \kappa}\right)\bar{U} \sim -\frac{\kappa}{y^3}\,, \quad \text{as} \quad y \to \infty\,. \tag{5.45}$$

A homogeneous solution $\bar{U}_h$ to this equation has decay $\bar{U}_h = \mathcal{O}(e^{-2\sqrt{2}|y|^{3/2}/3})$ as $y \to \infty$, whereas the particular solution $\bar{U}_p$ satisfies $\bar{U}_p = \mathcal{O}(y^{-4})$ as $y \to \infty$. This shows that any solution to (5.42) with $U_y \to -1$ as $y \to \infty$, has asymptotics

$$U \sim -\sqrt{y^2 - \kappa} + \mathcal{O}(y^{-4}) \sim -y + \frac{\kappa}{2y} + \mathcal{O}(y^{-2})\,, \qquad \text{as} \quad y \to \infty\,. \tag{5.46}$$

We then substitute (5.46) into (5.43) for A to obtain the following far-field behavior of the boundary-layer solution:

$$A \sim a_{0c} + \epsilon^{2/3} a_{0c} \beta^{1/2} \left(-y + \frac{\kappa}{2y}\right)\,.$$

Upon recalling that $y = \epsilon^{-2/3}\beta^{1/6}(\ell - x)$, the equation above yields the following matching condition for the outer solution:

$$A \sim a_{0c} + a_{0c}\beta^{1/2}(x - \ell) + \epsilon^{4/3}\left(\frac{a_{0c}\kappa\beta^{1/6}}{2}\right)\frac{1}{\ell - x}\,, \qquad \text{as} \quad x \to \ell^-\,. \tag{5.47}$$

Since the first two terms in (5.47) agree with the local behavior (5.30) as $x \to \ell^-$ of the renormalized outer solution

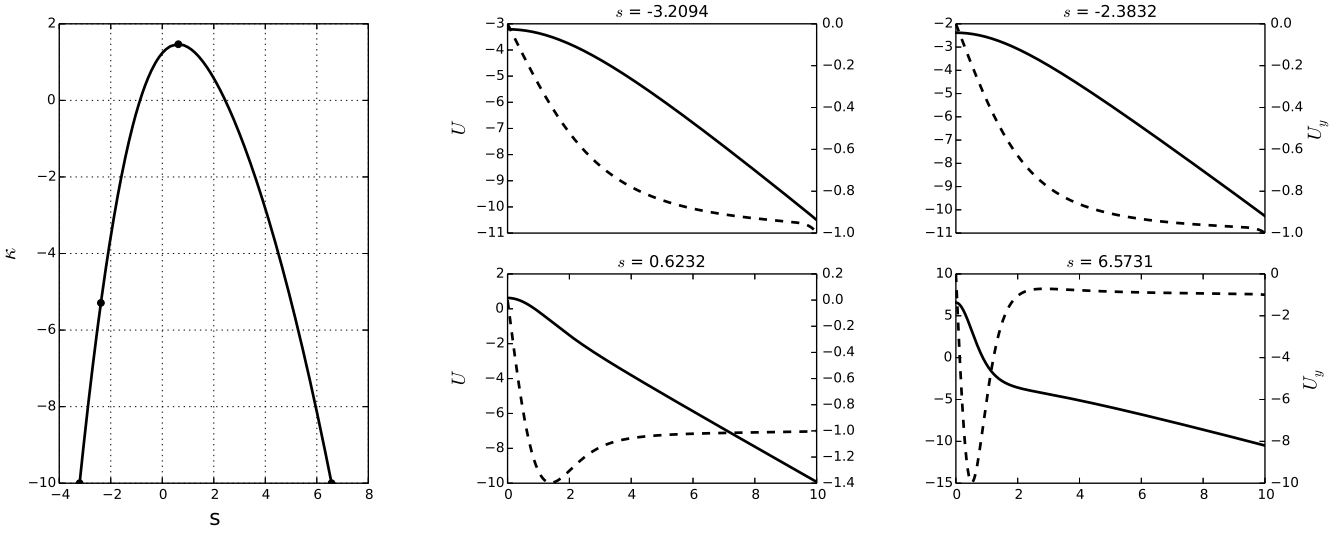

Figure 10. Left: Plot of the bifurcation diagram of κ versus $s = U(0)$ for solutions to the normal form equation (5.42). Right: the solution $U(y)$ (solid curves) and the derivative $U'(y)$ (dashed curves) versus y at four values of s on the bifurcation diagram.

$a_\epsilon(x)$, we obtain upon comparing (5.32) with (5.47) that

$$\nu \equiv \epsilon^{4/3}\,, \tag{5.48}$$

and that $a_{\epsilon,1}$ satisfies (5.34) subject to the singular behavior

$$a_{\epsilon,1} \sim \left(\frac{a_{0c}\kappa\beta^{1/6}}{2}\right)\frac{1}{\ell - x}\,, \qquad \text{as} \quad x \to \ell^-\,. \tag{5.49}$$

To solve (5.34) subject to (5.49) it is convenient to introduce the new variable $\tilde{a}_{\epsilon,1}$ defined by

$$\tilde{a}_{\epsilon,1} \equiv f(a_\epsilon)a_{\epsilon,1}\,.$$

Then, we calculate using (5.30), (5.49), and $f'(a_{0c}) = -2/a_{0c}^2$ that

$$\tilde{a}_{\epsilon,1} \sim f'(a_{0c})a_{0c}\beta^{1/2}(x-\ell)\left(\frac{a_{0c}\kappa\beta^{1/6}}{2}\right)\frac{1}{\ell - x} = \beta^{2/3}\kappa\,, \qquad \text{as} \quad x \to \ell^-\,.$$

Therefore, from this limiting behavior and (5.34), we conclude that $\tilde{a}_{\epsilon,1}$ satisfies

$$(\tilde{a}_{\epsilon,1})_{xx} - \frac{\Lambda_\epsilon}{f(a_\epsilon)}\tilde{a}_{\epsilon,1} = \Lambda_{\epsilon,1}a_\epsilon\,, \qquad x_\epsilon < x < \ell\,, \tag{5.50 a}$$

$$\tilde{a}_{\epsilon,1}(x_\epsilon) = 0\,; \qquad \tilde{a}_{\epsilon,1} \to \beta^{2/3}\kappa\,, \quad \text{as} \quad x \to \ell^-\,. \tag{5.50 b}$$

We observe that since $f(a_\epsilon) = 0$ has a simple zero at $x = \ell$, then $x = \ell$ is a regular singular point for the differential operator in (5.50 a). In (5.50) the condition at $x = \ell$ is over-determined in the sense that we are specifying that $\tilde{a}_{\epsilon,1}$ is bounded as $x \to \ell^-$ and that the limiting behavior of $\tilde{a}_{\epsilon,1}$ as $x \to \ell^-$ is a pre-specified constant. This extra implicit condition in the boundary condition at $x = \ell$ is the condition that determines $\Lambda_{\epsilon,1}$.

To determine $\Lambda_{\epsilon,1}$ it is convenient to reformulate (5.50) by introducing the new variable H by $\tilde{a}_{\epsilon,1} \equiv \Lambda_{\epsilon,1}H$, so that H satisfies

$$H_{xx} - \frac{\Lambda_\epsilon}{f(a_\epsilon)}H = a_\epsilon\,, \qquad x_\epsilon < x < \ell\,; \qquad H(x_\epsilon) = 0\,, \quad H \text{ bounded as } x \to \ell^-\,. \tag{5.51}$$

In terms of the solution to (5.51) we identify the constant H_ℓ from $H_\ell \equiv \lim_{x\to\ell^-} H(x)$. With H_ℓ now known, we

obtain upon comparing (5.51) with (5.50) that

$$\Lambda_{\epsilon,1} = \frac{\beta^{2/3}\kappa}{H_\ell}\,. \tag{5.52}$$

Our numerical computations below show that $H_\ell > 0$.

Finally, from (5.33) and (5.43), and the expression for β in (5.39), we obtain a local parametric description of the bifurcation diagram of $A(\ell)$ and D in the form

$$D \sim D_{\rm crit,\epsilon} - \epsilon^{4/3} D_{\rm crit,\epsilon}^{4/3}\left(\frac{(\gamma-\alpha)^{2/3}\kappa}{2^{2/3}H_\ell}\right), \qquad A(\ell) \sim a_{0c}\left(1+\epsilon^{2/3}\beta^{1/3}U(0)\right), \tag{5.53}$$

where $a_{0c} = 3\alpha/2$. Since the graph of κ versus $U(0)$ is multivalued from Fig. 10, we conclude from (5.53) that the graph of $A(\ell)$ versus D has a fold-point behavior near $D_{\rm crit,\epsilon}$. When $H_\ell > 0$, we observe from (5.53) and Fig. 10 that D attains its minimum value $D_{\min,\epsilon}$ when $\kappa = \kappa_{\max} \approx 1.466$, corresponding to $U(0) \approx 0.615$.

To numerically compute the constant H_ℓ, we use a shooting method after first formulating an asymptotic boundary condition to hold as $x \to \ell^-$. Near $x = \ell$, we calculate from (5.30) that

$$\frac{\Lambda_\epsilon}{f(a_\epsilon)} \sim \frac{r}{\eta}\,, \qquad r \equiv \frac{\Lambda_\epsilon a_{0c}}{2\beta^{1/2}}\,, \qquad \eta = \ell - x\,,$$

so that near $x = \ell$, (5.51) becomes

$$H_{\eta\eta} - \frac{r}{\eta}H = a_{0c} - \beta^{1/2}a_{0c}\eta + \cdots\,.$$

The local behavior of the solution is readily calculated as

$$H(\eta) \sim H_\ell\left[1 + r\eta\log\eta + \mathcal{O}(\eta)\right], \qquad \text{as} \quad \eta \to 0^+\,, \tag{5.54}$$

which, after eliminating H_ℓ, yields the asymptotic boundary condition

$$H_x \sim -rH\log(\ell - x)\,, \qquad \text{as} \quad x \to \ell^-\,. \tag{5.55}$$

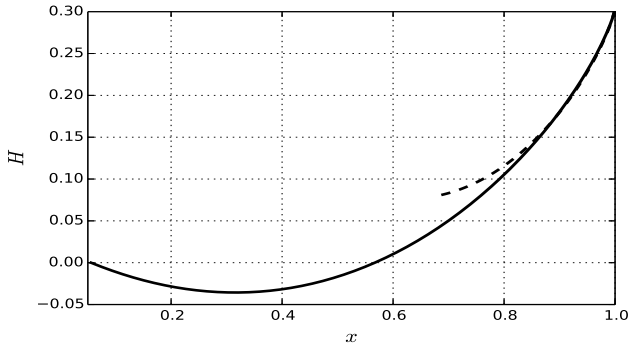

Figure 11. Numerically computed solution (solid curve) to (5.51) with asymptotic boundary condition (5.55) imposed at $x = \ell - \delta$, with $\delta = 0.000001$, and with parameter values $\gamma = 2$, $\alpha = 1$, $\ell = 1$, and $\epsilon = 0.01$. We obtain $H_\ell = \lim_{x\to\ell^-} H(x) \approx 0.303$. The dashed curve is the local Frobenius series approximation for H, valid near $x = \ell$, with leading terms given in (5.54).

To determine the constant H_ℓ we use a shooting method on (5.51), which consists of iterating on the constant H_0 in $H_x(x_\epsilon) = H_0$, and then imposing (5.55) at $x = \ell - \delta$, where δ with $0 < \delta \ll 1$ is a regularization parameter. The function $a_\epsilon(x)$ in (5.51) is determined by calculating $a_{\epsilon,x}$ from a first integral of (5.25). For $\gamma = 2$, $\alpha = 1$, and $\epsilon = 0.01$, our computations yield $H_\ell \approx 0.303$ when $\delta = 0.000001$, which yields $D_{\min,\epsilon} \approx 1.598$ from (5.53). In Fig. 11 we plot the numerically computed $H(x)$ versus x when $\gamma = 2$, $\alpha = 1$, $\ell = 1$, $\epsilon = 0.01$, and $H_\ell = 0.303$. The dashed curve in this plot is a local Frobenius series approximation valid near $x = \ell$, with leading terms given in (5.54).

For two values of ϵ, in Fig. 12 we show a favorable comparison between the asymptotic and full numerical results for A and V in the boundary layer region at the fold point value. The full numerical results are computed using `AUTO-07p`.

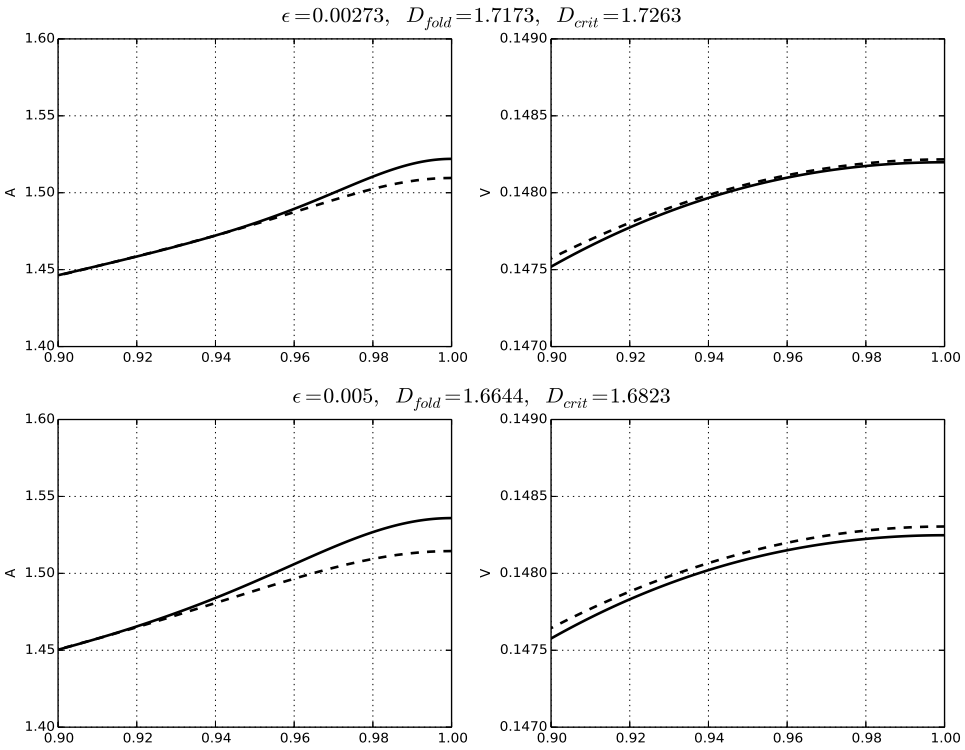

Figure 12. The asymptotic results (dashed curves) for A (left) and V (right) in the boundary layer region near $x = \ell$ at the fold point value for D are compared with corresponding full numerical results (solid curves). The asymptotic fold point value is given by (5.53). The top row is for $\epsilon = 0.00273$ and the bottom row is for $\epsilon = 0.005$. The other parameter values are $\gamma = 2$, $\alpha = 1$, and $\ell = 1$.

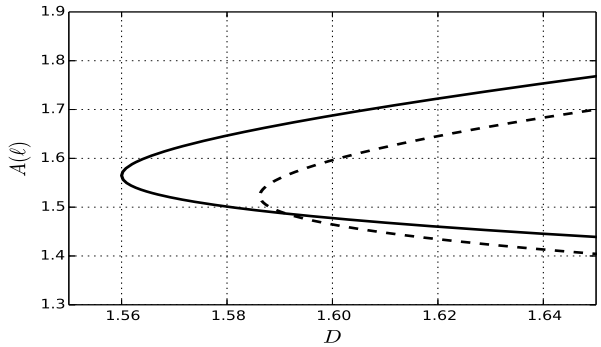

Figure 13. The asymptotic result (dashed curve) for $A(\ell)$ versus D in a narrow interval near the fold point, as obtained from (5.53) with $H_\ell \approx 0.303$, is compared with the corresponding full numerical result (solid curve) computed using `AUTO-07p`. The parameter values are $\gamma = 2$, $\alpha = 1$, $\ell = 1$, and $\epsilon = 0.01$.

Finally, in Fig. 13 we compare the asymptotic result (5.53) for $A(\ell)$ versus D, with $H_\ell \approx 0.303$, near the fold point with the corresponding full numerical result computed using `AUTO-07p`. The plot is a zoom of the region near the fold point.

6 An ODE-DAE System for the Slow Dynamics of Crime Hotspots

In this section we derive an ODE-DAE system for the slow dynamics of a collection of hotspots. In our analysis we assume that a quasi-steady pattern of localized hotspots has emerged from initial data by way of some transient process for (1.4). As such, we assume that we have "prepared" initial data consisting of a quasi steady-state hotspot pattern. The analysis below characterizing the slow evolution of the quasi steady-state hotspot pattern relies heavily on the refined asymptotic theory of §5. We first consider the dynamics of a single hotspot centered at x_0 in the domain $|x| \le \ell$. In §6.2 we extend the analysis to study the dynamics of a multi-hotspot pattern. In §6.3 we compare results from the asymptotic theory of slow hotspot dynamics with corresponding full numerical results.

6.1 The Slow Dynamics of One Hotspot

To characterize the slow dynamics of a single hotspot we proceed by adapting the analysis of §5. A dominant balance argument shows that the speed of the hotspot is $\mathcal{O}(\epsilon^2)$. In the inner region, where $y = \epsilon^{-1}(x - x_0(\sigma))$, with $\sigma = \epsilon^2 t$, we pose a two-term expansion for A as

$$A \sim A_0/\epsilon + A_1 + \dots , \qquad V \sim \epsilon^2 V_\epsilon \, .$$

Upon substituting this expansion into (1.4), and after retaining the dominant correction terms, we obtain that

$$\left(A_{0yy} - A_0 + V_\epsilon A_0^3\right) + \epsilon\left(A_{1yy} - A_1 + 3V_\epsilon A_0^2 A_1 + \alpha\right) + \cdots = -\epsilon \dot{x}_0 A_{0y} \, , \tag{6.1 a}$$

$$D\left[\left(A_0^2 + 2\epsilon A_0 A_1\right) V_{\epsilon y}\right]_y - \epsilon V_\epsilon\left(A_0^3 + 3A_0^2 A_1 \epsilon\right) + \epsilon^2(\gamma - \alpha) + \cdots = -\epsilon^3\left(A_0^2 V_\epsilon\right)_y \dot{x}_0 \, . \tag{6.1 b}$$

As in §5, we expand $V_\epsilon = V_0 + \epsilon V_1 + \cdots$ and substitute this expansion into (5.1) and collect powers of ϵ. This yields the leading-order result that V_0 is an unknown constant and that $A_0 = w/\sqrt{V_0}$, where $w(y) = \sqrt{2}\,\mathrm{sech}\, y$. At next order, in place of (5.3), we obtain on $-\infty < y < \infty$ that

$$L_0 A_1 \equiv A_{1yy} - A_1 + 3w^2 A_1 = -\alpha - \frac{V_1}{V_0^{3/2}} w^3 - \frac{w_y}{\sqrt{V_0}} \dot{x}_0 \, , \qquad \left[w^2 V_{1y}\right]_y = \frac{\sqrt{V_0}}{D} w^3 \, . \tag{6.2}$$

Since L_0 has a one-dimensional nullspace with $L_0 w_y = 0$, the solvability condition for the A_1-equation in (6.2) provides

$$\int_{-\infty}^{\infty} \left(\alpha w_y + \frac{V_1}{V_0^{3/2}} w^3 w_y + \frac{w_y^2}{\sqrt{V_0}} \dot{x}_0 \right) dy = 0 \, .$$

Since w is odd with $w(\pm\infty) = 0$, this condition reduces to

$$\dot{x}_0 \int_{-\infty}^{\infty} w_y^2 \, dy = -\frac{1}{4V_0} \int_{-\infty}^{\infty} V_1 \left(w^4\right)_y \, dy \, .$$

We integrate this expression by parts and use the fact that $w = \mathcal{O}(e^{-|y|})$ as $|y| \to \infty$, together with $V_1 = \mathcal{O}(e^{2|y|})$ as $|y| \to \infty$ (see the discussion below equation (5.3)), to eliminate the boundary term and obtain that

$$\dot{x}_0 \int_{-\infty}^{\infty} w_y^2 \, dy = \frac{1}{4V_0} \int_{-\infty}^{\infty} \left(w^2 V_{1y}\right) w^2 \, dy \, .$$

We then integrate this expression once more by parts to get

$$\dot{x}_0 \int_{-\infty}^{\infty} w_y^2 \, dy = \frac{1}{4V_0} \left[\left(w^2 V_{1y}\right) I(y) \Big|_{-\infty}^{\infty} - \int_{-\infty}^{\infty} \left(w^2 V_{1y}\right)_y I(y) \, dy \right] , \tag{6.3}$$

where $I(y) \equiv \int_0^y w^2 \, ds$. Since $I(y)$ is odd, and $\left(w^2 V_{1y}\right)_y$ is even in y from (6.2), it follows that the integral on the right-hand side of (6.3) vanishes identically. In addition, upon using $w = \sqrt{2}\,\mathrm{sech}\, y$, we can evaluate the integral ratio $\int_{-\infty}^{\infty} w^2 \, dy / \int_{-\infty}^{\infty} w_y^2 \, dy = 3$. In this way, (6.3) reduces to

$$\dot{x}_0 = \frac{3}{8V_0} \left[\lim_{y\to\infty} \left(w^2 V_{1y}\right) + \lim_{y\to-\infty} \left(w^2 V_{1y}\right) \right] . \tag{6.4}$$

The last step in the analysis is to evaluate the two limits in (6.4) by using the gradient information on V provided by the knee solution. The analysis of the mid-inner, knee, and outer solutions for A and V proceeds analogously as in §5, since these solutions are quasi-steady on the time-scale of the slow dynamics. As such, in our discussion below, we only highlight the results of the analysis.

In place of (5.25), the renormalized outer problem is now formulated as

$$D\left[f(a_\epsilon)a_{\epsilon x}\right]_x = a_\epsilon - \gamma\,, \qquad \text{on} \quad x_{0+\epsilon} < x < \ell\,, \quad -\ell < x < x_{0-\epsilon}\,, \tag{6.5 a}$$

$$a_\epsilon(x_{0+\epsilon}) = \alpha\,, \quad a_\epsilon(x_{0-\epsilon}) = \alpha\,, \quad a_{\epsilon x}(\pm\ell) = 0\,, \tag{6.5 b}$$

where $x_{0\pm\epsilon} > 0$ is defined by in terms of the hotspot location x_0 by

$$x_{0\pm\epsilon} \equiv x_0 \pm x_\epsilon \qquad x_\epsilon \equiv (-\epsilon\log\epsilon) + \epsilon\left(1 + \log\left(\frac{2\sqrt{2}}{\alpha}\right) - \log\sqrt{V_0}\right)\,. \tag{6.5 c}$$

In terms of $a_\epsilon(x)$, the renormalized outer solution $v_\epsilon(x)$ is

$$v_\epsilon(x) = g\left(a_\epsilon(x)\right)\,, \tag{6.6}$$

where $g(a)$ is defined in (2.4).

By matching the renormalized outer solution across the knee and mid-inner solutions one can obtain, as in §5, the gradient information for V_1 as $y \to \pm\infty$. More specifically, in place of (5.22), we obtain that

$$V_1 \sim b_\pm e^{2\pm y}\,, \quad \text{as} \quad y \to \pm\infty\,, \qquad b_\pm \equiv \pm\left(\frac{\alpha^2}{2c^2}\right) v_{\epsilon x}(x_{0\pm\epsilon})\,, \qquad c \equiv \frac{2\sqrt{2}}{\sqrt{V_0}}\,. \tag{6.7}$$

By using this limiting behavior, together with the asymptotics $w \sim 2\sqrt{2}e^{\pm y}$ as $y \to \pm\infty$, we can evaluate the two limits in (6.4) as

$$\lim_{y\to\pm\infty}\left(w^2 V_{1y}\right) = 8\lim_{y\to\pm\infty}\left(e^{\mp 2y}V_{1y}\right) = \alpha^2 V_0 v_{\epsilon x}(x_{0\pm\epsilon})\,. \tag{6.8}$$

Then, from (6.6) we calculate $v_{\epsilon x}(x_{0\pm\epsilon}) = \alpha^{-3}a_{\epsilon x}(x_{0\pm\epsilon})$, where we used $g'(\alpha) = \alpha^{-3}$. In this way, (6.4) reduces an ODE determined in terms of the renormalized outer solution $a_\epsilon(x)$, satisfying (6.5), given by

$$\dot{x}_0 = \frac{3}{8\alpha}\left[a_{\epsilon x}(x_{0+\epsilon}) + a_{\epsilon x}(x_{0-\epsilon})\right]\,. \tag{6.9}$$

By calculating a first integral of (6.5), as similar to that in (2.9), we readily derive that

$$a_{\epsilon x}(x_{0+\epsilon}) = \sqrt{\frac{2}{D}}\alpha\sqrt{G(\mu_+) - G(\alpha)}\,, \qquad a_{\epsilon x}(x_{0-\epsilon}) = -\sqrt{\frac{2}{D}}\alpha\sqrt{G(\mu_-) - G(\alpha)}\,, \tag{6.10}$$

so that (6.9) becomes

$$\frac{dx_0}{d\sigma} = \frac{3}{8}\sqrt{\frac{2}{D}}\left[\sqrt{G(\mu_+) - G(\alpha)} - \sqrt{G(\mu_-) - G(\alpha)}\right]\,, \qquad \sigma \equiv \epsilon^2 t\,. \tag{6.11 a}$$

Here $G(u)$ is defined in (2.8 b), and $\mu_\pm \equiv a_\epsilon(\pm l)$ are determined in terms of the hotspot location x_0 and the constant V_0 from the implicit relations

$$\chi(\mu_+) = \sqrt{\frac{2}{D}}\left(\ell - x_{0+\epsilon}\right)\,, \qquad \chi(\mu_-) = \sqrt{\frac{2}{D}}\left(\ell + x_{0-\epsilon}\right)\,, \tag{6.11 b}$$

where $\chi(\mu)$ is defined in (2.11). Finally, to derive the renormalized equation for V_0 we proceed as in (5.26) of §5, to obtain

$$D\alpha^2\left[v_{\epsilon x}(x_{0+\epsilon}) - v_{\epsilon x}(x_{0-\epsilon})\right] \sim \frac{1}{\sqrt{V_0}}\int_{-\infty}^{\infty} w^3\,dy - 2x_\epsilon(\gamma - \alpha)\,.$$

By substituting $v_{\epsilon x}(x_{0\pm\epsilon}) = \alpha^{-3}a_{\epsilon x}(x_{0\pm\epsilon})$, and using (6.10), we solve the resulting expression for V_0 to get the approximate equation

$$V_0 = \frac{2\pi^2}{\left[\sqrt{2D}\left(\sqrt{G(\mu_+) - G(\alpha)} - \sqrt{G(\mu_-) - G(\alpha)}\right) + 2x_\epsilon(\gamma - \alpha)\right]^2}\,. \tag{6.11 c}$$

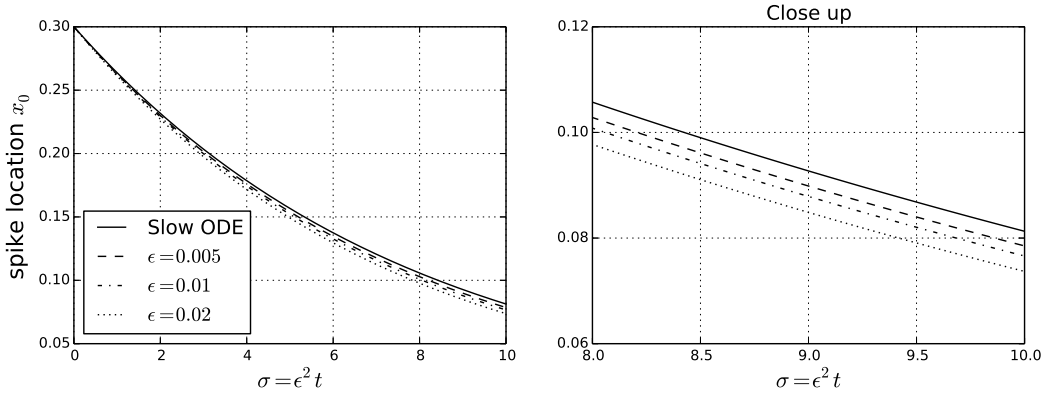

Figure 14. For parameter values $\gamma = 2$, $\alpha = 1$, $\ell = 1$, $D = 4$, and with initial state $x_0(0) = 0.3$, the asymptotic result (6.11) for slow hotspot dynamics is plotted for three values of ϵ. These results are compared with the corresponding result when the switchback term $-\epsilon \log \epsilon$ is neglected, so that $x_{0\pm\epsilon} = x_0$ in (6.11 *b*). The plot on the right is a zoom of that on the left.

For a given x_0, (6.11 *b*) and (6.11 *c*) are a weakly nonlinear algebraic system for $\mu_\pm$ and V_0, where the coupling arises through the weak dependence of x_ϵ on V_0. With $\mu_\pm$ determined in this way for a given x_0, the speed of the hotspot when at location x_0 is given by (6.11 *a*). In this sense, the system (6.11) is a differential-algebraic ODE system for the evolution of a single hotspot, starting from some initial value $x_0(0)$ with $|x_0(0)| < \ell$.

For the solvability of (6.11 *b*) and (6.11 *c*), corresponding to the existence of an outer solution, we require that the domain lengths for the two outer solutions on either side of x_0 not exceed a threshold. In particular, as similar to that in (2.14) of §2, we require that the following constraint, guaranteeing that no new hotspot is nucleated or created at the domain boundaries, is satisfied:

$$\max\{l + x_{0-\epsilon}, l - x_{0+\epsilon}\} \le \ell_{\max}\,, \qquad \ell_{\max} \equiv \sqrt{\frac{D}{2}}\chi_{\max}\,, \qquad \chi_{\max} \equiv \chi\,(3\alpha/2)\ . \tag{6.12}$$

We now discuss a key qualitative feature of the dynamics (6.11). Our main observation is that the dynamics of a single hotspot is symmetrizing in the sense that

$$\begin{cases} \dot{x}_0 < 0 & \text{if } x_0 > 0 \\ \dot{x}_0 > 0 & \text{if } x_0 < 0 \end{cases}\,, \tag{6.13}$$

so that the hotspot is repelled from the domain boundaries. To see this, we note that if $x_0 < 0$, then from (6.11 *b*) and the fact that $\chi(\mu)$ is monotone increasing in μ, it follows that $\mu_- < \mu_+$. Then, since $G(u)$ is monotone increasing in u, we conclude that $G(\mu_-) < G(\mu_+)$, so that $\dot{x}_0 > 0$ from (6.11 *a*). As a result of this symmetrizing property of the hotspot dynamics, it follows that if the constraint (6.12) is satisfied for the initial hotspot location $x_0(0)$, then this constraint will still hold for all time under the DAE evolution (6.11). This implies that no new hotspots can be nucleated at later times near the domain boundaries under the slow dynamics of a single hotspot. Since $x_{0e} = 0$ is the only fixed point of the dynamics, we have that $x_0 \to 0$ as $\sigma \to \infty$ for any $x_0(0)$.

In Fig. 14 we show the quantitative effect on the slow hotspot dynamics of the switchback term $-\epsilon \log \epsilon$. Recall that in (6.11 *b*), $x_{0\pm\epsilon}$ is defined in terms of this switchback term by (6.5 *c*). With the initial value $x_0(0) = 0.3$, the asymptotic result for the slow dynamics of x_0 versus $\sigma = \epsilon^2 t$ is plotted for three values of ϵ, and is compared with the corresponding result when the swtichback term is not included, so that $x_{0\pm\epsilon} = x_0$ in (6.11 *b*).

We remark that although the DAE dynamics (6.11) for x_0 is highly nonlinear when $D = \mathcal{O}(1)$, it simplifies considerably in the limit $D \gg 1$. For $D \gg 1$, we can approximate the solution to the renormalized problem (6.5) by

$$a_\epsilon = \alpha + \frac{1}{D}\tilde{a}_\epsilon + \cdots\,,$$

where $\tilde{a}_\epsilon$ satisfies

$$\tilde{a}_{\epsilon xx} = \frac{(\alpha-\gamma)}{f(\alpha)} = \alpha(\alpha-\gamma)\,, \qquad x_{0+\epsilon} < x < \ell\,, \quad -\ell < x < x_{0-\epsilon}\,,$$
$$\tilde{a}_\epsilon(x_{0\pm\epsilon}) = 0\,, \quad \tilde{a}_{\epsilon x}(\pm\ell) = 0\,.$$

From the simple solution to this limiting problem, we calculate for $D \gg 1$ that

$$a_{\epsilon x}(x_{0+\epsilon}) \sim \frac{1}{D}\alpha(\alpha-\gamma)(x_{0+\epsilon}-\ell)\,, \qquad a_{\epsilon x}(x_{0-\epsilon}) \sim \frac{1}{D}\alpha(\alpha-\gamma)(x_{0-\epsilon}+\ell)\,. \tag{6.14}$$

By substituting (6.14) into (6.9), we obtain the following simple linear ODE dynamics, with flow towards the origin, for a one-hotspot solution when $D \gg 1$:

$$\dot{x}_0 \sim -\frac{3}{4D}(\gamma-\alpha)x_0\,. \tag{6.15}$$

6.2 A DAE System for Repulsive Hotspot Dynamics

In this section we generalize the results for the dynamics of a single hotspot to the case where there are $N \geq 1$ hotspots on the domain $|x| \leq \ell$. We label the centers of the hotspots by x_j for $j = 1, \ldots, N$, and assume the ordering $-\ell < x_1 < x_2 < \cdots < x_N < \ell$. In order to simplify our analysis, we will use the leading-order result that the spatial extent of the hotspot centered at x_j is $x_j - x_\epsilon < x < x_j + \epsilon$, where $x_\epsilon = -\epsilon\log\epsilon + \mathcal{O}(\epsilon)$. By neglecting the $\mathcal{O}(\epsilon)$ term in x_ϵ and using $x_\epsilon \sim -\epsilon\log\epsilon$ the slow hotspot dynamics becomes uncoupled from the heights of the hotspots. With this simplification, the adjacent outer problems for the hotspots centered x_j and x_{j+1} must agree at a common vanishing Neumann boundary point at the midpoint $(x_j + x_{j+1})/2$. With this observation, and by using translation invariance of (1.4), it is clear that the one-hotspot results derived above can be readily adapted to determine the dynamics of a collection of hotspots.

More precisely, let ℓ_{j+} and ℓ_{j-} denote the half-lengths of the outer problems on either side of the hotspot centered at x_j for $j = 2, \ldots, N-1$. In contrast, for the hotspot adjacent to $x = -\ell$, we let ℓ_{1-} be the distance from x_1 to $x = -\ell$, whereas ℓ_{N+} is the distance from x_N to $x = \ell$. In terms of x_j, this yields

$$\ell_{j+} \equiv \frac{(x_{j+1}-x_j)}{2}\,, \quad j = 1, \ldots, N-1\,; \quad \ell_{j-} \equiv \frac{(x_j - x_{j-1})}{2}\,, \quad j = 2, \ldots, N\,; \quad \ell_{N+} = \ell - x_N\,, \quad \ell_{1-} = l + x_1\,. \tag{6.16 a}$$

We then define the constants μ_{j+} and μ_{j-} for $j = 1, \ldots, N$ by the implicit equations

$$\chi(\mu_{j+}) = \sqrt{\frac{2}{D}}\left[\ell_{j+} - (-\epsilon\log\epsilon)\right]\,, \qquad \chi(\mu_{j-}) = \sqrt{\frac{2}{D}}\left[\ell_{j-} - (-\epsilon\log\epsilon)\right]\,. \tag{6.16 b}$$

In terms of the $\mu_{j\pm}$, which depend on the instantaneous locations of the hotspots, the centers of the N hotspots satisfies the slow dynamics

$$\dot{x}_j \sim \frac{3}{8}\sqrt{\frac{2}{D}}\left(\sqrt{G(\mu_{j+}) - G(\alpha)} - \sqrt{G(\mu_{j-}) - G(\alpha)}\right)\,, \qquad j = 1, \ldots, N. \tag{6.16 c}$$

The DAE system (6.16) for the slow evolution of a collection of hotspots is valid provided that the lengths of the outer regions between adjacent hotspots is below a threshold, i. e. provided that

$$\max_{j=1,\ldots,N}\{\ell_{j-}, \ell_{j+}\} \leq \ell_{\max}\,, \qquad \ell_{\max} \equiv \sqrt{\frac{D}{2}}\chi_{\max}\,, \qquad \chi_{\max} \equiv \chi\left(3\alpha/2\right)\,. \tag{6.17}$$

A steady-state configuration for the N-hotspot pattern is the equally-spaced solution whereby

$$x_j = -\ell + \frac{(2j-1)}{N}\ell\,, \qquad j = 1, \ldots, N\,.$$

6.3 Comparison of Asymptotic and Full Numerical Results for Slow Hotspot Dynamics

Finally, we compare the asymptotic results (6.11) and (6.16) for slow hotspot dynamics with corresponding full numerical results computed using the software `PDEPE` in `MATLAB R2013b`. For the full numerical computations, we take

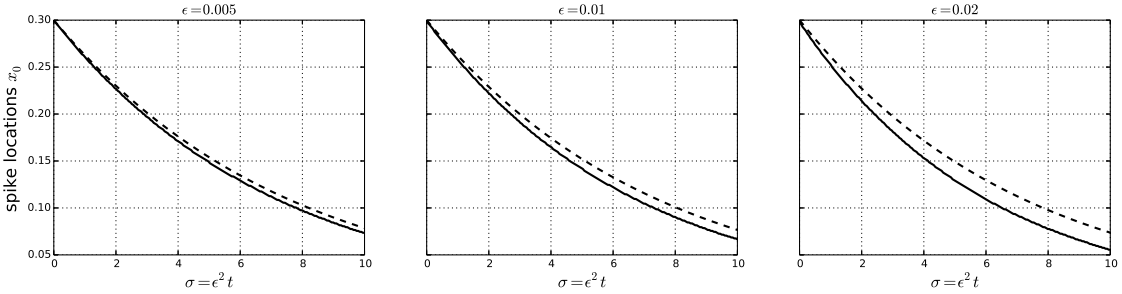

Figure 15. The slow dynamics of a single hotspot on the slow time-scale σ, as predicted by the asymptotic theory (6.11) (dashed curves), are compared with corresponding full numerical results of the PDE system (1.4) (solid curves) computed using `PDEPE` of `MATLAB R2013b`. The domain is $|x| \leq 1$ and the parameter values are $\gamma = 2$, $\alpha = 1$, and $D = 4$. Left: $\epsilon = 0.005$. Middle: $\epsilon = 0.01$. Right: $\epsilon = 0.02$.

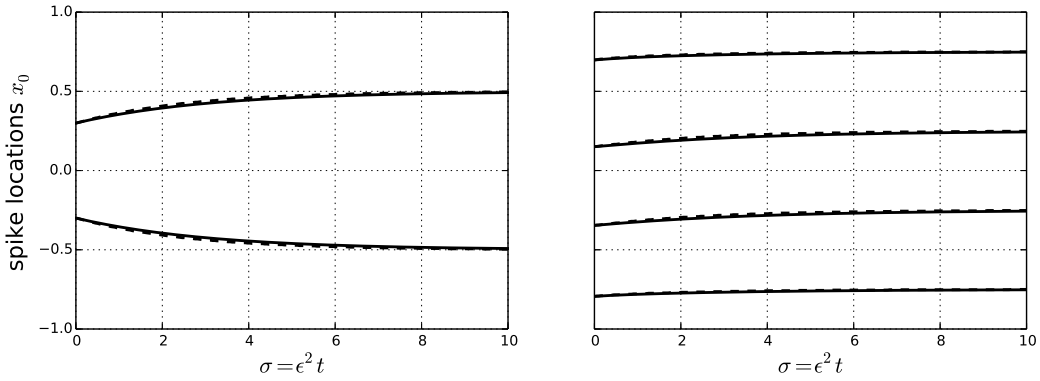

Figure 16. Comparison of slow dynamics predicted from the asymptotic theory (6.16) (dashed curves) and from full numerical simulations (solid curves) of the PDE system (1.4). The domain is $|x| \leq 1$ and the parameter values are $\gamma = 2$, $\alpha = 1$, and $\epsilon = 0.01$. Left: a two-hotspot evolution with $D = 2$, with initial locations $x_0 \approx -0.300$, 0.299. Right: a four-hotspot evolution with $D = 0.3$, with initial locations are $x_0 \approx -0.794$, -0.346, 0.151, 0.698.

$10/\epsilon + 1$ evenly-spaced spatial meshpoints in order to adequately resolve the narrow cores of the hotspots. Initial conditions for the quasi steady-state hotspot patterns are generated by evolving the PDE (1.4) from small initial bump perturbations, such as shown in the left panel of Fig. 2. The resulting transient evolution leads to the formation of a pattern of hotspots that is essentially stationary on $\mathcal{O}(1)$ time intervals. The locations of the maxima of A for this pattern are then identified numerically. We re-initialize the full numerical computations by using this computed hotspot pattern as the initial condition for (1.4). Then, the subsequent slow evolution of the maxima of A are tracked numerically over very long time intervals, and compared with corresponding results from the asymptotic theory.

In Fig. 15 we compare the asymptotic results for the slow dynamics of a single hotspot, as predicted by (6.11), with corresponding full numerical results. The comparisons are done for three values of ϵ. The agreement between the asymptotic and numerical results is very close when $\epsilon = 0.005$, but is still decent even when $\epsilon = 0.02$.

For the case of multiple hotspots, and with $\epsilon = 0.01$, in Fig. 16 we show a very favorable comparison between the slow dynamics predicted from the asymptotic theory (6.16) and that computed numerically from the full PDE system (1.4) for either a two or four hotspot evolution.

7 Discussion

We conclude this paper by briefly discussing a few possible directions for further research. A first open direction is to analyze hotspot dynamics for some extensions of the basic 1-D model (1.4). Possible extensions of the basic model include, allowing for spatial variability of the rate at which criminals are re-introduced, so that $\gamma - \alpha$ depends on x,

accounting for the effect of crime deterrence by police presence (cf. [**28**], [**40**]), or allowing for a nonlinear diffusivity of the attractiveness field (cf. [**13**]).

A key open problem is to extend the preliminary analysis in [**21**] to analyze the existence, stability, and dynamics of 2-D localized hotspot patterns to (1.1) in the limit $\epsilon \to 0$ with $D = \mathcal{O}(1)$ on bounded 2-D domains. For simpler RD systems, without the chemotactic term in the inhibitor variable as in (1.1), such as the Gierer-Meinhardt, Schnakenberg, and Gray-Scott systems, results in 2-D for the slow dynamics of localized solutions are given in [**17**], [**19**], and [**8**] (see also the references therein).

In §5 of [**21**], a formal asymptotic analysis was used in the limit $\epsilon \to 0$, and with $D \gg 1$, to construct quasi steady-state patterns of $K \geq 1$ well-separated hotspots for (1.1) in arbitrary, but bounded, 2-D domains. Through the derivation and analysis of a nonlocal eigenvalue problem, it was shown in [**21**] that, on the $D \gg \mathcal{O}(1)$ regime, a one-hotspot pattern is linearly stable on an $\mathcal{O}(1)$ time-scale. Additionally, it was shown that K-hotspot patterns with $K \geq 2$ are linearly stable on an $\mathcal{O}(1)$ time-scale when $D < \epsilon^{-4} D_{0c}/K^3$, where D_{0c} depends on γ, α and the area of the domain. Therefore, for multi-hotspot patterns on the regime $D \gg \mathcal{O}(1)$, the stability threshold occurs when $D = \mathcal{O}(\epsilon^{-4})$. No study of the slow dynamics of 2-D hotspot patterns was made in [**21**].

The mathematical challenge with analyzing the $D = \mathcal{O}(1)$ regime in 2-D is that, in contrast to the 1-D case studied herein, the outer problem for the attractiveness field will consist of a nonlinear elliptic PDE that cannot be reduced to a simple quadrature. However, we do expect that this nonlinear PDE has a saddle-node bifurcation structure and leads to a peak insertion phenomena, similar to that studied in 1-D. Furthermore, the characterization of the slow dynamics of a collection of hotspots should depend on the spatial gradient of the solution to the nonlinear outer problem at the hotspot locations. The goal would be to investigate whether it is possible in 2-D that new hotspots can be nucleated through peak-insertion events that are triggered, intermittently in time, from the overall collective dynamics of interacting hotspots. Such a mechanism, if it exists, would give rise to highly complex spatio-temporal patterns of dynamically interacting hotspots, similar to that found for the chemotaxis-growth model of [**27**] in one spatial dimension.

Acknowledgements

M. J. W. gratefully acknowledges the grant support of NSERC (Canada).

References

[1] H. Berestycki, J. Wei and M. Winter (2014), *Existence of symmetric and asymmetric spikes for a crime hotspot model*, SIAM J. Math. Anal., **46**(1), pp. 691–719

[2] P. L. Brantingham, P. J. Brantingham (1987), *Crime Patterns*, McMillan.

[3] J. Burke and E. Knobloch (2007), *Homoclinic snaking: Structure and Stability*, Chaos, **17**, 037102.

[4] V. Brena-Medina and A. Champneys (2014), *Subcritical Turing bifurcation and the morphogenesis of localized patterns*, Phys. Rev. E., **90**, 032923.

[5] R. Cantrell, C. Cosner and R. Manasevich (2012), *Global bifurcation of solutions for crime modeling equations*, SIAM J. Math. Anal., **44**(3), pp. 1340–1358.

[6] W. Chen and M. J. Ward (2009), *Oscillatory instabilities and dynamics of multi-spike patterns for the one-dimensional Gray-Scott model*, Europ. J. Appl. Math **20**(2), pp. 187–214.

[7] L. Chen, N. Goldenfeld and Y. Oono (1994), *Renormalization group theory for global asymptotic analysis*, Phys. Rev. Lett., **73**(10), pp. 1311-1315.

[8] W. Chen and M. J. Ward (2011), *The stability and dynamics of localized spot patterns in the two-dimensional Gray-Scott model*, SIAM J. Appl. Dyn. Sys., **10**(2), pp. 582–666.

[9] E. J. Doedel and B. Oldeman (2009), AUTO07P: continuation and bifurcation software for ordinary differential equations. Technical report, Concordia University, 2009

[10] A. Doelman, R. A. Gardner and T. J. Kaper (2001), *Large stable pulse solutions in reaction-diffusion equations*, Indiana U. Math. J., **50**(1), pp. 443–507.

[11] A. Doelman and T. J. Kaper (2003), *Semistrong pulse interactions in a class of coupled reaction-diffusion systems*, SIAM J. Appl. Dyn. Sys., **2**(1), pp. 53–96.

[12] A. Doelman, T. J. Kaper and K. Promislow (2007), *Nonlinear asymptotic stability of the semi-strong pulse dynamics in a regularized Gierer-Meinhardt model*, SIAM J. Math. Anal., **38**(6), pp. 1760–1789.

[13] Y. Gu, Q. Wang and G. Yi (2014), *Stationary patterns and their selection mechanism of Urban crime models with heterogeneous near-repeat victimization effect*, preprint, arXiv:1409.0835.

[14] D. Iron and M. J. Ward (2002), *The dynamics of multi-spike solutions to the one-dimensional Gierer-Meinhardt model*, SIAM J. Appl. Math., **62**(6), pp. 1924–1951.
[15] D. Iron, M. J. Ward and J. Wei (2001), *The stability of spike solutions to the one-dimensional Gierer-Meinhardt model*, Physica D, **150**(1-2), pp. 25–62.
[16] S. Johnson and K. Bower (2005), *Domestic burglary repeats and space-time clusters: The dimensions of risk*, Europ. J. of Criminology, **2**, pp. 67–92.
[17] T. Kolokolnikov and M. J. Ward (2003), *Reduced-wave Green's functions and their effect on the dynamics of a spike for the Gierer-Meinhardt model*, Europ. J. Appl. Math., **14**(5), pp. 513–545.
[18] T. Kolokolnikov, M. J. Ward and J. Wei (2005), *The existence and stability of spike equilibria in the one-dimensional Gray-Scott model: The low feed-rate regime*, Studies in Appl. Math., **115**(1), pp. 21–71.
[19] T. Kolokolnikov, M. J. Ward and J. Wei (2009), *Spot self-replication and dynamics for the Schnakenburg model in a two-dimensional domain*, J. Nonlinear Sci., **19**(1), pp. 1–56.
[20] T. Kolokolnikov, M. J. Ward, and J. Wei (2007), *Self-replication of mesa patterns in reaction-diffusion models*, Physica D, **236**(2), pp. 104–122.
[21] T. Kolokolnikov, M. J. Ward and J. Wei (2014), *The stability of steady-state hot-spot patterns for a reaction-diffusion model of urban crime*, DCDS-B, **19**(5), p. 1373–1410.
[22] P. Lagerstrom (1988), *Matched asymptotic expansions: ideas and techniques*, Applied Mathematical Sciences, **76**, Springer-Verlag, New York.
[23] P. Lagerstrom and D. Reinelt (1984), *Note on logarithmic switchback terms in regular and singular perturbation problems*, SIAM J. Appl. Math., **44**(3), pp. 451–462.
[24] A. Lindsay and M. J. Ward (2010), *Asymptotics of some nonlinear eigevalue problems for a mems capacitor: Part II: Multiple solutions and singular asymptotics*, Europ. J. Appl. Math., **22**(2), pp. 83–123.
[25] W. Liu, A. L. Bertozzi, and T. Kolokolnikov (2012), *Diffuse interface surface tension models in an expanding flow*, Comm. Math. Sci., **10**(1), pp. 387–418.
[26] D. J. B. Lloyd and H. O'Farrell (2013), *On localised hotspots of an urban crime model*, Physica D, **253**, pp. 23–29.
[27] K. Painter and T. Hillen (2011), *Spatio-temporal chaos in a chemotaxis model*, Physica D, **240**, pp. 363–375.
[28] A. B. Pitcher (2010), *Adding police to a mathematical model of burglary*, Europ. J. Appl. Math., **21**(4-5), pp. 401–419.
[29] N. Popovic and P. Szymolyan (2004), *A geometric analysis of the Lagerstrom model problem*, J. Diff. Eq.erential Equations, **199**(2) pp. 290–325.
[30] J. D. M. Rademacher (2013), *First and second order semi-strong interaction in reaction-diffusion systems*, SIAM J. Appl. Dyn. Syst., **12**(1), pp. 175–203.
[31] N. Rodriguez and A. Bertozzi (2010), *Local existence and uniqueness of solutions to a PDE model for criminal behavior*, M3AS (special issue on Mathematics and Complexity in Human and Life Sciences), **20**(1), pp. 1425–1457.
[32] M. B. Short, M. R. D'Orsogna, V. B. Pasour, G. E. Tita, P. J. Brantingham, A. L. Bertozzi and L. B. Chayes (2008), *A statistical model of criminal behavior*, Math. Models. Meth. Appl. Sci., **18**, Suppl. pp. 1249–1267.
[33] M. B. Short, A. L. Bertozzi and P. J. Brantingham (2010), *Nonlinear patterns in urban crime - hotspots, bifurcations, and suppression*, SIAM J. Appl. Dyn. Sys., **9**(2), pp. 462–483.
[34] M. B. Short, P. J. Brantingham, A. L. Bertozzi and G. E. Tita (2010), *Dissipation and displacement of hotpsots in reaction-diffusion models of crime*, Proc. Nat. Acad. Sci. **107**(9) pp. 3961-3965.
[35] W. Sun, M. J. Ward and R. Russell (2005), *The slow dynamics of two-spike solutions for the Gray-Scott and Gierer-Meinhardt systems: competition and oscillatory instabilities*, SIAM J. Appl. Dyn. Syst., **4**(4), pp. 904–953.
[36] M. J. Ward and J. Wei (2003), *Hopf bifurcations and oscillatory instabilities of spike solutions for the one-dimensional Gierer-Meinhardt model*, J. Nonlinear Sci., **13**(2), pp. 209–264.
[37] J. Wei (1999), *On single interior spike solutions of the Gierer–Meinhardt system: uniqueness and spectrum estimates*, Europ. J. Appl. Math., **10**(4), pp. 353–378.
[38] J. Wei (2008), *Existence and stability of spikes for the Gierer-Meinhardt system*, book chapter in *Handbook of Differential Equations, Stationary Partial Differential Equations*, Vol. 5 (M. Chipot ed.), Elsevier, pp. 489–581.
[39] J. Q. Wilson and G. L. Kelling (1998), *Broken windows and police and neighborhood safety*, Atlantic Mon., **249**, pp. 29–38.
[40] J. R. Zipkin, M. B. Short and A. L. Bertozzi (2014), *Cops on the dots in a mathematicsl model of urban crime and police response*, DCDS B, **19**(5), pp. 1479–1506.